Taurine as a key intermediate for host-symbiont interaction in the tropical sponge *Ianthella basta*

Florian U. Moeller[1], Craig W. Herbold[1], Arno Schintlmeister[1,2], Maria Mooshammer[1], Cherie Motti[3], Faris Behnam[1], Margarete Watzka[4], Thomas Schweder[5,6], Mads Albertsen[7], Andreas Richter[4], Nicole S. Webster[3,7,8], and Michael Wagner[1,2,9]

[1]Centre for Microbiology and Environmental Systems Science, Division of Microbial Ecology, University of Vienna, Austria

[2]Large-Instrument Facility for Environmental and Isotope Mass Spectrometry, Centre for Microbiology and Environmental Systems Science, University of Vienna, Vienna, Austria

[3]Australian Institute of Marine Science, Townsville, Queensland, Australia

[4]Centre for Microbiology and Environmental Systems Science, Division of Terrestrial Ecosystem Research, University of Vienna, Austria

[5]Institute of Marine Biotechnology e.V., Greifswald, Germany

[6]Institute of Pharmacy, Pharmaceutical Biotechnology, University of Greifswald, Greifswald, Germany

[7]Australian Centre for Ecogenomics, School of Chemistry and Molecular Biosciences, University of Queensland, St Lucia, Queensland, Australia

[8]Australian Antarctic Division, Kingston, Tasmania, Australia

[9]Center for Microbial Communities, Department of Chemistry and Bioscience, Aalborg University, Aalborg, Denmark

Abstract

Marine sponges are critical components of marine benthic fauna assemblages where their filter-feeding and reef-building capabilities provide bentho-pelagic coupling and crucial habitat. As potentially the oldest representation of a metazoan-microbe symbiosis, they also harbor dense, diverse, and species-specific communities of microbes which are increasingly recognized for their contributions to dissolved organic matter (DOM) uptake. Recent omics-based studies of marine sponge microbiomes have proposed numerous pathways of dissolved metabolite exchange between the host and symbionts within the context of the surrounding environment, but few studies have sought to experimentally interrogate these pathways. By using a combination of metaproteogenomics and laboratory incubations coupled with isotope-based functional assays, we showed that the dominant gammaproteobacterial symbiont '*Candidatus* Taurinisymbion ianthellae' residing in the marine sponge, *Ianthella basta*, expresses a pathway for the import and dissimilation of taurine, a ubiquitously occurring sulfonate metabolite in marine sponges. '*Candidatus* Taurinisymbion ianthellae' incorporates taurine-derived carbon and nitrogen while at the same time oxidizing the dissimilated sulfite into sulfate for export. Furthermore, we found that taurine-derived ammonia is exported by the symbiont for immediate oxidation by the dominant ammonia-oxidizing thaumarchaeal symbiont '*Candidatus* Nitrosospongia ianthellae'. Metaproteogenomic analyses also indicate that '*Candidatus* Taurinisymbion ianthellae' likely imports DMSP and possesses both pathways for DMSP demethylation and cleavage enabling it to use this compound as a carbon and sulfur source for biomass as well as for energy conservation. These results highlight the important role of biogenic sulfur compounds in the interplay between *Ianthella basta* and its microbial symbionts.

Introduction

Marine sponges are important components of coral reefs with a range of critical ecological functions [1]. Sponges play a crucial role in maintaining biomass in reef ecosystems by filtering dissolved organic matter (DOM) from large quantities of water and capturing it as biomass, which is then shed as particulate organic matter (POM) and passed to higher trophic levels [2–4]. Marine sponges often harbor dense, diverse and stable communities of microorganisms that are thought to play a role in DOM capture as well as a broad suite of other nutrient transformations [3, 5, 6]. These microbial symbionts have been shown to photosynthetically fix carbon [7], fix N_2 [8], nitrify [9, 10], as well as carry out anammox, denitrification, and sulfate respiration [11, 12]. Furthermore, isotope labeling experiments have proven that symbiont-derived carbon and nitrogen can be found in sponge cells [7, 11, 13–15]

Whilst the specificity, biogeography and environmental sensitivity of the relationship between sponges and their microbiome has been intensively studied [16–18], our understanding of the physiological interactions between sponges and their symbiotic microorganisms is still very limited. Genome-based investigations of the sponge microbiome have revealed an array of diverse metabolic potential encoded in symbiont genomes, including the processing of organic carbon, nitrogen and sulfur compounds [19–22], autotrophic sulfur oxidation [23, 24], and vitamin synthesis [25, 26]. These metabolic processes may be mediated by a diverse array of transporters encoded in the symbionts to facilitate exchange with the host as well as the surrounding environment (reviewed in [27]). In a few studies, metaproteomic analyses have revealed the expression of proteins indicative of metabolic interactions between the host and symbionts, including transport functions for typical sponge metabolites and the potential mediation of host-symbiont interactions via the expression of eukaryotic-like proteins and cell-cell mediators [10, 28]. Despite these insights obtained from a variety of approaches, the high complexity of sponge holobionts coupled with the inherent difficulty in culturing sponge symbionts has made it challenging to irrevocably link host interactions and symbiont physiology with symbiont phylogeny.

One way of examining host-symbiont interaction is by tracking compounds that may be shared between them, such as taurine. Taurine has been reported from a broad suite of sponge species, oftentimes as one of the

most abundant free amino acids (up to 74% of the free amino acid pool; [29]). Free-living marine bacteria can utilize taurine produced by phytoplankton [30–32] and the genetic capacity for taurine utilization has been identified in marine sponge microbiomes [23, 24, 33–35]. Taurine is an ideal osmoregulator as it is transported by a Na^+-dependent transport system unique to β-amino acids and so it is responsive to ionic activities and other osmotic agents [36, 37]. As a zwitterionic compound, extremely high intra- to extracellular concentration gradients for taurine can be maintained, and due to its lipophobic properties, it is not readily lost by diffusion [38]. Taurine also likely functions as a storage and transport compound, providing nitrogen and sulfur to symbionts in the gutless clams *Solemya reidi* [39] and *Solemya velum* [40]. The synthesis of sulfur-containing free amino acids has long been proposed as a strategy for sulfide detoxification and transport in chemoautotrophic symbioses [41–45] and taurine is the dominant free amino acid in many of these species [39, 41–45].

Ianthella basta [46] is a widely distributed sponge species found throughout the Indo-Pacific region [47]. In contrast to many marine sponge species with high microbial abundance of microbial symbionts [48], *I. basta* hosts only a low diversity of microbial symbionts being dominated by three phylotypes including an Alphaproteobacterium, a Gammaproteobacterium and a Thaumarchaeote, which all occur at relatively high abundances in the sponge mesohyl [10, 49, 50]. This 'low complexity' community is highly stable across different host morphotypes [51], across the large geographic range of the host, under different host health states [50] and across a wide suite of environmental conditions [52]. Thus, the *I. basta* holobiont represents a comparatively tractable model system for the investigation of sponge-symbiont physiological interactions. Recently, we were able to demonstrate that the thaumarchaeal symbiont of *I. basta* – "*Candidatus* Nitrosospongia ianthellae" – is an active ammonia oxidizer and that, surprisingly, this sponge does not harbor a bacterial nitrite oxidizer [10]. However, the physiology of the remaining two symbiont phylotypes remains unknown. In this study, we elucidate key physiological traits of the gammaproteobacterial *I. basta* symbiont, which we named "Candidatus Taurisymbion ianthellae". Based on annotation of the metagenome-assembled genome (MAG) of this symbiont, we focused on the important biogenic sulfonate intermediate, taurine. We document the expression of a previously described [53] but infrequently observed pathway for the transport and

dissimilation of taurine into sulfite, followed by sulfite oxidation into sulfate encoded by the symbiont, and provide experimental physiological support for this sponge-microbe interaction.

Material and methods

Sponge collection for metaproteogenomics and I. basta holobiont taurine incubations. Two large adult specimens of the purple thick morphotype of the sponge *Ianthella basta* were collected in waters offshore from Orpheus Island (18°36.878'S, 146°29.990'E), Queensland, Australia, in October 2010 and 2011 and processed as described in [10] for metaproteogenomic analysis. In addition, sponge clones were used for 48-hour batch incubations either in the presence or absence of taurine. The sponge clones used for the taurine incubations were derived from a single large yellow thin morph *Ianthella basta* individual with collected from Davies Reef (18°49.354 S, 147°38.253 E) on 21st November 2014. Upon collection, the individual was maintained in flow-through reef seawater onboard the RV Cape Ferguson until its return to the Australian Institute of Marine Science (AIMS) where the individual was cut into small sponge clones (approx. 5 cm x 5 cm 0.5 cm) and left to heal in AIMS aquaria overnight. Live sponge clones were then transferred to sulfate-free artificial seawater (SFASW) and rinsed 3 times to remove as much sulfate from seawater as possible. For all incubation experiments, *I. basta* clones were incubated at 25ºC in the dark in acid-washed glass tanks either filled with 0.2 µm natural filtered seawater (FSW) or SFASW, and with or without taurine added at different time points and concentrations. All incubations were conducted in the dark to preclude light inhibition of nitrification. SFASW incubations were conducted to more readily discern the production of sulfate from the taurine-dissimilation/sulfite oxidation pathway since natural seawater contains sulfate at high concentrations. In the first set of experiments, 1 mM unlabeled taurine was added at the beginning of the incubations and another 0.6 mM pulse was added at t = 36 h. For stable isotope incubations in standard seawater, ^{15}N and ^{13}C labeled taurine (2-Amino-^{15}N-ethanesulfonic acid: Taurine-^{15}N, 98 atom%; 2-Aminoethane-$^{13}C2$-sulfonic Acid: Taurine-$^{13}C2$, 99 atom%; Campro Scientific GmbH, Berlin, Germany) were added in equimolar concentrations simultaneously, so as to monitor potential incorporation into *I. basta* holobiont biomass as well as to track dissimilation into NH_4^+, followed by successive oxidation to NO_2^- by the dominant thaumarchaeal symbiont [10]. For these two sets of

experiments, incubations were conducted in closed 1 l acid-washed glass aquaria under static conditions at room temperature and water sampling occurred at t = 0, 12, and 48 h, while sampling of *I. basta* biological material occurred at the end of the experiment at t = 48h. Additionally, two follow-up experiments were conducted in SFASW in closed 250 ml acid-washed glass aquaria but with higher temporal resolution (t = 0, 12, 24, 36, and 48 h) and 1 mM or 100 µM isotopically unlabelled taurine added at the beginning of the incubation. Finally, to determine whether the resultant and pronounced increase in NH_4^+ in the taurine incubation experiments affects sulfate production rates of the holobiont, 48 h incubations (sampling at t = 0, 12, and 48 h) were conducted with *I. basta* holobiont clones in either only in SFASW, in SFASW amended with 100 µM NH_4^+, and solely in freshwater (FW), respectively. Freshwater incubations were conducted as a control for the production of sulfate during elicited host stress resulting from reduced salinity conditions. For all sets of incubations excluding the experiment at elevated NH_4^+ concentrations, parallel control incubations were performed under identical conditions but without *I. basta* clones. All incubations were conducted in triplicates.

For chemical analyses, seawater samples (10 ml) were taken from the containers (see above-described set of experiments) and filtered using 0.45 µm Sartorius Minisart cellulose acetate filters (Göttingen, Germany). Duplicate samples for dissolved inorganic nitrogen (NH_4^+, NO_2^-, NO_3^-) were measured on a Seal AA3 segmented flow analyser and referenced against OSIL standards and in-house reference samples. Sulfate was measured via ion chromatography, followed by detection via suppressed conductivity. Confirmation of taurine uptake by *I. basta* was established following a two-step pre-column fluorometric derivatization HPLC method adapted from [54]. o-Phthalaldehyde-ethanethiol (OPA-ET; Sigma Aldrich; 750 µl), prepared daily in methanol (MeOH; Sharlau) buffered with 0.8 M borate (Sigma Aldrich; pH11) and aged at 4°C for 2 h, was added to 100 µL of seawater sample diluted in 900 µl MilliQ H_2O. After 1 min, 50 µl of fluorenylmethyloxycarbonyl chloride (FMOC-Cl [Sigma Aldrich], prepared in acetonitrile [Sharlau] and pre-aged >12 h, was added; the higher concentration of the derivatizing reagents was required to ensure complete reaction of the taurine (~mM). After a further 1 min, 10 µl of the derivatized sample was injected onto an Agilent 1100 HPLC system (comprising a binary pump, autosampler, column oven and fluorescence detector, operated using Chemstation for LC 3D Rev. A.10.01 and 735 Sampler Software v6.10). Samples (n=2 samples per treatment per timepoint; n=5 replicate

injections per sample) were chromatographed on a 250 mm× 4.6 mm i.d., 5 μm particle size, HILIC (Phenomenex) column under the following conditions: 1 ml min^{-1} flow rate; column maintained at 40°C; mobile phases comprising MeOH-sodium acetate (0.36 M; pH 7.0)-H_2O (55:8:37, v/v/v) (A) and acetonitrile-sodium acetate (0.36 M; pH 7.0)-H_2O (10:5:85, v/v/v) (B); gradient 15% A at 0–2 min, 15–20% A at 2–6 min, 40% A at 6–9 min, 85% A at 9–17 min then held until 20 min; the column was flushed with 100% A at 20-21 min and held for a further 4 min before re-equilibration at 15% A for 5 min; fluorescence detection (excitation: 330 nm, emission: 460 nm). For calibration, a taurine stock solution (1 M; >99.9% Sigma Aldrich) was prepared in Milli-Q water and a dilution series prepared (10 mM – 1 nM). γ-Aminobutyric acid (5 M GABA; Sigma Aldrich) was used as the internal standard. The dilution series was stored at 4°C. The calibration curve (R^2 = 0.99) was used to quantify taurine in seawater. ^{15}N-analyses of ammonium and nitrite from the incubation experiments with stable-isotope labeled taurine are described below.

Cryosectioning and FISH for relative symbiont quantification. The aforementioned *I. basta* individual collected for metagenomic sequencing in October 2010 was assayed for its microbiological composition using fluorescence *in situ* hybridization (FISH). Briefly, after sample collection, the *I. basta* specimen was cut into tissue strips of approximately 4 cm^3, fixed in 4% paraformaldehyde (PFA) for 1 h at room temperature and stored in ethyl alcohol (EtOH)-phosphate-buffered saline (PBS) (1:1) at -20ºC. For FISH, PFA-fixed samples of *I. basta* were embedded in Neg-50 (Richard-Allan Scientific), a cryogenic water-soluble sectioning medium, and cut to 4-μm thin sections (Leica CM3050 S). We designed specific 16S rRNA-targeted FISH probes for the visualization of '*Ca*. Taurinisymbion ianthellae' (GamD1137, 5'-CTC AAA GTC CCC GCC ATT-3') and the dominant alphaproteobacterial symbiont (AlfD729, 5`-CGGACCTGGCGGCCGCTT-3'). To calculate the relative abundance of '*Ca*. Taurinisymbion ianthellae', we applied the double-labeled FISH probe GamD1137 (Cy3), along with the double-labeled FISH probe for the α-symbiont (AlfD729 in Fluos) and the double-labeled probe mix EUB338-I, EUB338-II, and EUB338-III (all in Cy5; [55]) in equimolar concentrations. *I. basta* sponge section hybridizations were carried out in the presence of 25% formamide in the hybridization buffer (after formamide concentration optimization), and the stringency of the washing buffer was adjusted accordingly

[56]. As a negative control, the nonsense probe called nonEUB338-I (reverse complementary probe to EUB338-I; double labeled in FLUOS, Cy3, and Cy5) was applied on one section per well per slide hybridized [57]. Probe-conferred visualizations of fluorescent cells were carried out by a confocal laser scanning microscope (CLSM) (LSM 510 Meta; Zeiss, Oberkochen, Germany). Specifically labelled bacterial cells were counted by eye in 10 randomly selected fields of view (each field containing an average of 260.6 ± 73 SD cells of '*Ca*. Taurinisymbion ianthellae' at 630X magnification), and the fraction of '*Ca*. Taurinisymbion ianthellae' relative to total bacterial cells stained by the EUB338 probe mix was calculated.

DNA extraction from whole sponge tissue and qPCR for symbiont quantification. Between 80-150 mg of *I. basta* sponge tissue was thawed (if previously frozen at -80 ºC), rinsed successively (3x) in 1X calcium- and magnesium-free artificial seawater (CMF-ASW) and immediately ground into a paste with a mortar and pestle in liquid N_2. After resuspension in TE buffer, DNA was extracted from the suspension using the same methods as described in [10] for DNA extraction prior to symbiont quantification via quantitative PCR (qPCR). DNA was extracted from the two individuals used for metaproteogenomics (see above) as well as three additional yellow thin morphotype healthy individuals from a previous study examining the persistence of microbial symbionts in diseased and healthy specimens of *I. basta* (Luter *et al*., 2010). qPCR was used to quantify the number of 16S rRNA genes of '*Ca*. Taurinisymbion ianthellae', the thaumarchaeal ammonia-oxidizer '*Ca.* Nitrosospongia ianthellae', and the dominant α-proteobacterial symbiont using specific primers designed for each symbiont phylotype in [10].

NMR-, LC-MS-based detection and quantification of taurine in Ianthella basta.

To establish the presence of taurine in *I. basta*, a section of tissue from a yellow thin morphotype was excised by scalpel, weighed wet, and exhaustively extracted with 90% MeOH in MilliQ water. The MeOH extract was lyophilized overnight (Dynavac Freeze-drier). The dry MeOH extract (~5 mg) was dissolved in 1 mL deuterated methanol (CD_3OD; Cambridge Isotope Laboratories) for analysis by proton nuclear magnetic resonance (^1H NMR; Bruker Avance 600 MHz, 5 mm CPTXI inverse ^1H-^{13}C/^{15}N Z-gradient cryogenically cooled probe,

referenced to CD_3OD 3.31 ppm, standard 1D zg pulse sequence). Given the crude nature of the extract and the likelihood that the diagnostic signals would be unable to be distinguished from similar chemistry in the extract, 20 mg (dissolved in ~1 mL 50% MeOH) was chromatographed over a pre-equilibrated Strata C18-E 55 μm, 70Å, 1000 mg solid phase extraction cartridge (C18-SPE; Phenomenex) and eluted with 10 mL of H_2O, 10% MeOH, 50% MeOH and 100% MeOH. The four fractions (Fr 1-4) were evaporated under nitrogen stream at 40°C and lyophilized to dryness. Fr 1-2 were prepared in 100% deuterated H_2O (D_2O; Cambridge Isotope Laboratories; referenced at 4.39 ppm) and Fr 3-4 in 10% CD_3OD: 90% CD_3OD (referenced to 3.31 ppm) and analysed by ^1H NMR. ^1H and COSY NMR spectra of 100 μM taurine standard, prepared in D_2O, was used to confirm identification of taurine in Fr 1. Final confirmation was provided by spiking the ^1H NMR sample with 32 μl and 128 μl 100 μM taurine and measuring the increase via integration of the two triplet signals.

To corroborate the NMR assignment, Fr 1 was also analysed by LCMS. A 10 μl aliquot of the aqueous Fr 1 was injected onto an Agilent 1100 HPLC system coupled to a Bruker Esquire 3000 Quadrupole Ion Trap LCMS and eluted from a 150 mm x 3 mm Luna 5μ NH_2 (Phenomenex) column under the following conditions: 0.8 mL min^{-1} flow rate; column maintained at 40°C; mobile phases comprised of H_2O + 0.1 % formic acid (A) and MeOH + 0.1% formic acid (B); isocratic elution at 90% A: 10% B for 10 min. The ionspray voltage was set to -4500 V, declustering potential -500V, curtain gas flow 9 L min^{-1}, ion source gas 40 PSI, and spray temperature at 350°C. Data was acquired over the mass range 70-200 *m/z*; product ion MS/MS data was acquired over 50-200 *m/z* to establish the fragmentation pattern. Retention time and total and extracted ion chromatographs (positive mode) were compared against a 100 μM taurine standard prepared in MilliQ.

The concentration of taurine in sponge tissue was measured by quantitative NMR (qNMR) following [58]. Briefly, five sponge clone samples were extracted and chromatographed over C18-SPE as described above. ^1H NMR spectra of Fr 1 (~16 mg dry extract) from each of the five sponge extracts were acquired in 800 μl D_2O (δH 4.39) at 298 K, with sweep width 12 ppm (7184 Hz), 90° pulse, 35 sec relaxation delay, receiver gain 16, 2 dummy scans, 16 acquisition scans and 64 k data points. The external reference signal was calibrated using a stock solution of 2 mM taurine in D_2O. The concentration of taurine in the NMR samples was determined by

comparing the signal integrals of well resolved non-exchangeable protons (2H) centred at 3.26 ppm in a 0.20 ppm window with that of the reference signal. Concentration was normalized to wet weight of sponge (wet wt).

Isotopic analysis of whole sponge tissue, total nucleic acids, and ^{15}N in NH_4^+ & NO_2^- using EA-IRMS. For the determination of ^{13}C- and ^{15}N-enrichment within the holobiont, sponge tissue samples were rinsed briefly 3X in 1X CMF-ASW, freeze-dried, ground to a fine powder in a mortar, and stored dry prior to analysis. $\delta^{13}C$- and $\delta^{15}N$-values of sponge tissues were determined by an elemental analyzer (EA 1110, CE Instruments, Milan, Italy) coupled to an isotope ratio mass spectrometer (IRMS; Finnigan MAT Delta^{Plus} IRMS with a Finnigan MAT ConFlo III interface). For determination of ^{13}C- and ^{15}N-enrichment in total nucleic acids, *I. basta* whole sponge tissue was homogenized using the above procedure employing liquid N_2, followed by nucleic acid extraction according to the procedures outlined in [59]. The extracted nucleic acids were then dried overnight in an oven, and $\delta^{13}C$- and $\delta^{15}N$-values were determined via the same procedure as above. For quantification of the amount of ^{13}C- and ^{15}N-derived taurine that was incorporated into *I. basta* holobiont biomass the following formulas were used:

$$n_{C,taurine} = \frac{a_{^{13}C,sponge} - a_{^{13}C,ctrl}}{a_{^{13}C,taurine} - a_{^{13}C,ctrl}} \times n_{C,total}$$

$$n_{N,taurine} = \frac{a_{^{13}C,sponge} - a_{^{13}C,ctrl}}{a_{^{13}C,taurine} - a_{^{13}C,ctrl}} \times n_{C,total}$$

where the displayed symbols, abbreviations and designations refer to: *a* – isotope fraction $^{13}C/(^{12}C+^{13}C)$ or $^{15}N/(^{14}N+^{15}N)$ given in at%, *n*: number of carbon or nitrogen elemental atoms, *sponge* – sponge material; *ctrl* – natural isotope abundance control; *total* – total amount of carbon or nitrogen in the analyzed sample. For comparability of the measurement values obtained from distinct incubations, *n* was normalized to the wet weight of the utilized *I. basta* clones.

For ^{15}N-analysis of NH_4^+ and NO_2^-, sampled seawater from the glass tanks with the labeled taurine incubations was filtered through pre-combusted GF/Fs (Whatman International; treated for 4 h at 450˚C), and subsequently through 0.2 µm polycarbonate filters (Sartorius). All samples were immediately frozen at -20 ºC

for later analysis. Prior to shipment to the University of Vienna, samples were thawed at room temperature and the microbial inhibitor phenylmercuric acetate was added (to a final concentration of 10 µM). Upon arrival in Vienna the samples were promptly stored at -80ºC. For determination of the ^{15}N content in ammonia, NH_4^+ was extracted from samples via microdiffusion as described in [10] and following the protocol from [60]. Briefly, 100 mg MgO and an acid trap (acidified cellulose filter disc enclosed in a semi-permeable Teflon membrane) were added to 9 ml of sample and 1.5 ml of 3 M KCl. After 5 days shaking at 35°C, the acid traps were removed, dried over concentrated sulfuric acid and analyzed for the ^{15}N content by an elemental analyzer (EA 1110, CE Instruments, Milan, Italy) coupled to an isotope ratio mass spectrometer (IRMS; Finnigan MAT Delta^{Plus} IRMS with a Finnigan MAT ConFlo III interface). The nitrogen isotope composition of NO_2^- was determined by a method based on the reduction of NO_2^- to N_2O by using sodium azide under acidified conditions following the protocol of [61]. Briefly, 1 ml sample or standard was transferred to 12-ml exetainer and 1ml 1M HCl was added. After purging the vials with helium to expel air-N_2O from the sample headspace, 150 µl 1M sodium azide buffer (in 10% acetic acid solution) was injected and the vials were placed on a shaker at 37 °C for 18 h. The reaction was quenched by injecting 250 µl of 10M NaOH. Derived N_2O was analyzed using a purge-and-trap GC/IRMS system (PreCon, GasBench II headspace analyzer, Delta Advantage V IRMS; Thermo Fischer). Equivalently to the above calculations, the amount of taurine-derived NH_4^+ and NO_2^- were calculated as follows:

$$n_{NH_4^+,taurine} = \frac{a_{15N,\,NH_4^+} - a_{15N,ctrl}}{a_{15N,taurine} - a_{15N,ctrl}}\, n_{NH_4^+,total}$$

$$n_{NO_2^-,taurine} = \frac{a_{15N,\,NO_2^-} - a_{15N,ctrl}}{a_{15N,taurine} - a_{15N,ctrl}}\, n_{NO_2^-,total}$$

By taking into account that the isotopically labeled nitrite emerges from oxidation of ammonia obtained from taurine dissimilation, the total amount of NH_4^+ released by the holobiont through taurine metabolization was calculated via:

$$n_{NH_4^+,released} = \left(n_{NH_4^+,taurine,sponge} - n_{NH_4^+,taurine,SW}\right) + \left(n_{NO_2^-,taurine,sponge} - n_{NO_2^-,taurine,SW}\right)$$

where SW refers to the values determined from control incubations utilizing seawater without sponge clones. For comparability of the measurement values obtained from distinct incubations, *n* was normalized to the wet weight of the utilized *I. basta* clones.

NanoSIMS analysis of Ianthella basta. NanoSIMS measurements were undertaken on two of the three *I. basta* clone samples obtained from the $^{13}C^{15}N$-taurine incubations. Specimens were selected for maximum isotope enrichment, based on results from EA-IRMS bulk analysis (0.62 and 0.55 at% ^{15}N; 1.19 and 1.15 at% ^{13}C). Briefly, approximately 0.5 cm^3 sections were cut from *I. basta* samples which had been fixed in 4% PFA and stored in a 1:1 mixture of PBS and 96% ethanol at -20º C. The thus obtained specimens were then rinsed successively (3x) in 1X calcium- and magnesium-free artificial seawater (CMF-ASW) and gently dissociated in 1X CMF-ASW with a scalpel, mortar and pestle, and a final step of sonication for two 30 second cycles at 35% power using a sonication probe [Sonopuls HD2200 equipped with probe MS73 (output frequency 20 kHz, power 200 W, amplitude: 310 µm), Bandelin, Germany]. The suspensions were then filtered through 0.45 µm cellulose acetate filters (type Minisart, Sartorius, Göttingen, Germany) to remove a large portion of remaining sponge cells and nuclei (microscopic visualizations showed a lack of sponge nuclei after filtration), centrifuged at 10,844 × g for 10 min at 4°C to pellet cells, and resuspended in 50% EtOH/50% 1X PBS solution. To visualize all DNA-containing cells present in the sample, a 30 µL aliquot of the suspension was spotted onto antimony-doped silicon wafer platelets (7.1 x 7.1 x 0.75 mm; Active Business Company, Germany) and dried at 46º C, before staining with a 0.1 % (w/v) solution of the DNA-binding dye 4,6-diamidino-2-phenylindole (DAPI) (Sigma, Deisenhofen, Germany) at room temperature for 5 min. Excess DAPI was removed by rinsing with distilled water and the slides were air-dried. Samples were then imaged on an epi-fluorescence laser microdissection microscope (LMD, Leica LMD 7000) using a 40× air objective for pre-selection of suitable NanoSIMS measurement areas, which were subsequently marked utilizing the LMD laser. High resolution imaging of fluorescent cells in marked regions was carried out by a confocal laser scanning microscope (CLSM) (LSM 510 Meta; Zeiss, Oberkochen, Germany).

NanoSIMS measurements were performed on a NanoSIMS 50L (Cameca, Gennevilliers, France) at the Large-Instrument Facility for Environmental and Isotope Mass Spectrometry at the University of Vienna. Prior to data acquisition, analysis areas were pre-sputtered utilizing a high-intensity, slightly defocused Cs^+ ion beam (400 pA beam current, ~1 µm spot size) until a Cs^+ fluence of 3.2E15 ions cm^{-2} was obtained. Data were subsequently acquired as multilayer image stacks by sequential scanning of a finely focused Cs^+ primary ion beam (*ca*. 80 nm probe size at 2 pA beam current) over areas between 10.3 × 15 and 29 × 29 μm^2 at 176 × 256 and 512 × 512 pixel image resolution and a primary ion beam dwell time of 10 to 40 msec $(pixel*cycle)^{-1}$, corresponding to a per-cycle Cs^+ fluence in the range from 8.0E13 to 1.5E16 ions cm^{-2} per cycle. $^{12}C^-$, $^{13}C^-$, $^{12}C^{12}C^-$, $^{12}C^{13}C^-$, $^{12}C^{14}N^-$, $^{12}C^{15}N^-$, $^{31}P^-$ or $^{32}S^-$, as well as secondary electrons, were detected simultaneously. Signal intensities were corrected for detector dead time and quasi-simultaneous arrival (QSA) effects using QSA sensitivity factors (i.e., "beta" values) of 1.1, 1.1, 1.06, 1.06, 1.05, 1.05, 1.1, 1.1 for $^{12}C^-$, $^{13}C^-$, $^{12}C^{12}C^-$, $^{12}C^{13}C^-$, $^{12}C^{14}N^-$, $^{12}C^{15}N^-$, $^{31}P^-$, and ^{32}S, respectively.

Images based on NanoSIMS measurement data were generated using the Open MIMS plugin [62] in the FIJI package based on ImageJ [63]. C isotope composition images displaying the $^{13}C/(^{12}C+^{13}C)$ isotope fraction, designated as atom% ^{13}C, were inferred from the C_2^- secondary ion signal intensity distribution images via per-pixel calculation of $^{13}C^{12}C^-/(2\cdot^{12}C^{12}C^-+^{13}C^{12}C^-)$ intensity ratios, while N isotope composition images displaying the $^{15}N/(^{14}N+^{15}N)$ isotope fraction, designated as atom% ^{15}N, were inferred from the $^{12}CN^-$ secondary ion signal intensity maps via per-pixel calculation of $^{12}C^{15}N^-/(^{12}C^{15}N^-+^{12}C^{14}N^-)$ intensity ratios. Secondary electron images were utilized for representation of the sample morphology.

Region of interest (ROI) specific numerical data evaluation was also conducted using the Open MIMS plugin. ROIs were defined according to the isotope enrichment patterns since it was not possible to unambiguously identify characteristic cellular features. This was likely because analysis areas were accessed via depth-profiling, which is less suited for visualization of cellular (ultra)structure than e.g., cross-sectional analysis of resin embedded samples. C and N isotope compositions were calculated from the accumulated intensities of $^{12}C^{12}C^-$ and $^{12}C^{13}C^-$ and $^{12}C^{14}N^-$ and $^{12}C^{15}N^-$ secondary ion signals detected within each ROI. The isotopic composition values shown in Fig. S7 were determined via stepwise inspection of the isotopic enrichment patterns displayed in each individual image of the acquired multilayer stacks (Fig. S8). As such, the displayed

values may rather be considered as conservative estimates of the isotopic enrichment due to carry-over (e.g., through re-deposition and/or atomic mixing) of atoms and molecules from less enriched regions within the sponge extracellular matrix during the measurement process (including pre-sputtering). The analytical uncertainty of the isotope composition values (indicated by the error bars in Fig. S7), emerging from the random error in single ion counting, was estimated on the basis of Poisson statistics and calculated from the signal intensities (given in total counts within individual ROIs) via:

atom% ^{13}C inferred from C_2^- signal intensities:

$$\sigma_{\text{Pois, at\%13C}}=100/(2\cdot {}^{12}C^{12}C^- + {}^{12}C^{13}C^-)^2 \cdot \text{sqrt}(({}^{12}C^{12}C^-)^2 \cdot {}^{12}C^{13}C^- + ({}^{12}C^{13}C^-)^2 \cdot {}^{12}C^{12}C^-)$$

atom% ^{15}N inferred from CN^- signal intensities:

$$\sigma_{\text{Pois, at\%15N}}=100/({}^{12}C^{14}N^- + {}^{12}C^{15}N^-)^2 \cdot \text{sqrt}(({}^{12}C^{14}N^-)^2 \cdot {}^{12}C^{15}N^- + ({}^{12}C^{15}N^-)^2 \cdot {}^{12}C^{14}N^-)$$

Metagenome assembly and genome binning. Metagenome reads in fastq format, obtained from the Illumina sequencing runs, were end-trimmed at a minimum phred score of 15, a minimum length of 50 bp, allowing no ambiguous nucleotides and Illumina sequencing adaptors removed. Trimmed reads from each dataset were assembled using Spades version 3.11.0 [64], using default parameters and genomes were binned using Metabat v 2.12.0 [65]. MAGs from multiple Illumina datasets were dereplicated using dRep [66] and provisionally classified using CheckM [67]. A single high-quality gammaproteobacterial MAG was recovered after dereplication and uploaded to MaGe [68] for annotation. This MAG has been submitted to the European Nucleotide Archive with the accession number ERZ13292699 under BioProject PRJEB29556.

Two additional MAGs were assembled and binned from paired end reads from SRA runs derived from two sponge species, belonging to the same family as *Ianthella basta* (*Hexadella dedritifera* and *Hexadella* cf. *dedritifera*) [69]. Paired end reads for SRA runs SRR8088660, SRR8088661, SRR8088662 and SRR8088663 were downloaded from NCBI. BBduk (bbmap v. 37.61) was used to remove adapters and residual phiX (adapters.fa, phix174_ill.ref.fa.gz, ktrim=r k=21 mink=11 hdist=2), then quality filtered (minlen=99 qtrim=r trimq=15). Read sets were denoised using BayesHammer (SPAdes v3.15.3) [64] and merged using bbmerge (bbmap v. 37.61). Reads were assembled using SPAdes v3.15.3 (-k 21,33,55,77 --only-assemble) and

metaspades (-k 21,33,55,77 --only-assemble) resulting in 8 assemblies (2 assemblers, 4 datasets). Each read set was mapped against each assembly using bbmap v. 37.61(minid=0.99 idfilter=0.99 ambiguous=best pairedonly=t killbadpairs=t mappedonly=t) for and MAGs were generated using metabat1 and metabat2 algorithms (metabat v 2.15). MAGs from each SRA run were then dereplicated with dRep v 1.4.3 dereplicate_wf (-comp 40 -con 10 -l 200000) [66]. "Winning" MAGs from each SRA run were combined and dereplicated using dRep v 1.4.3 (-comp 40 -con 10 -l 200000 -pa 0.6 --S_algorithm gANI --S_ani 0.965). Reads from each SRA run were remapped to each MAG using bbmap v. 37.61(minid=0.99 idfilter=0.99 ambiguous=best pairedonly=t killbadpairs=t mappedonly=t and relative abundance was calculated by dividing mapped fragments by total fragments for each metagenomic dataset.

Phylogenetic analyses. Sequences for the '*Ca*. Taurinisymbion ianthellae' 16S rRNA species tree were assembled by merging a subset of sequences described by [70], along with top BLAST hits from representative gammaproteobacterial sequences, and the 16S rRNA sequences from the most closely related members with sequenced genomes. These sequences were aligned via the SINA aligner and the phylogenetic trees constructed in IQ-Tree, version 1.6.2 [71] using the model TN+F+R6 (after model selection using Model Finder; [72] with 10,000 ultrafast bootstraps (UFBoot, [73]). In addition, 16S rRNA gene sequences related to '*Ca*. Taurinisymbion ianthellae' were identified in short read archive (SRA) datasets using IMNGS (www.imngs.org, [74]) with default parameters. Successfully mapped reads were then aligned to the reference alignment using SINA and placed into the reference tree using the Evolutionary Placement Algorithm (EPA; [75]) implemented in RAxML-HPC 8.2.11 [76]. Phylogenomic reconstruction was based on a concatenated amino-acid alignment of 43 marker genes constructed with CheckM [67] and trees were constructed using the model LG+F+R7 (after model selection using Model Finder; [72]) with 1000 ultrafast bootstraps (UFBoot, [73]).

Proteomics. Proteome analysis was performed as done previously [10]. In brief, protein extracts were separated by 1D PAGE followed by liquid chromatography-based mass spectrometry (1D-PAGE-LC-MS/MS). MS spectra and MS/MS spectra were acquired from eluting peptides in a LTQ Orbitrap Velos hybrid mass

spectrometer (Thermo Fisher Scientific, Waltham, MA, USA), as described previously [77, 78] and searched against predicted protein sequence databases composed of the *I. basta* symbiont-enriched metagenome bins and common laboratory contaminants using the Sorcerer SEQUEST (v.27, rev. 11) algorithm. Protein identifications were filtered with Scaffold version 3.5.1 as described previously [79]. For protein identification only peptides identified with high mass accuracy (maximum ± 10 ppm difference between calculated and observed mass) were considered and at least two exclusively unique peptides were required to identify a protein. False-discovery rates (FDRs) were estimated with searches against a target-decoy database [80, 81]. For relative quantitation of proteins, normalized spectral abundance factors (NSAF) were calculated for each sample according to the method of [82] and averaged for all replicates and samples. The proteomics raw data have been deposited to the ProteomeXchange Consortium via the PRIDE partner repository with the dataset identifier PXD012484 and 10.6019/PXD012484.

Results and Discussion

A metagenome assembled genome and phylogenetic analyses of the dominant γ-proteobacterial symbiont of Ianthella basta

From the extensive metagenomic data set used in [10] for genomically characterizing the thaumarchaeal symbiont of *I. basta*, we retrieved a 2.35 Mbp MAG consisting of 97 contigs, representing a nearly complete genome (94.8%) with a very low level of contamination (Table S1). Phylogenetic analysis of the only 16S rRNA gene copy in the MAG demonstrated that this gene specifically clustered at 99% nucleotide identity with previously recovered sequences of the dominant gammaproteobacterial symbionts from *I. basta* (Fig. S1) [10, 50, 51] and fall into the neighborhood of sponge specific clusters 144-148 (SC) [70]. A phylogenomic reconstruction using concatenated single copy conserved marker genes (Fig. 1) [67], confirmed the affiliation of this MAG with the Gammaproteobacteria and revealed that it can be further classified into the Arenicellales order and within the LS-SOB family (originally named after the bacterial MAG extracted from the glass sponge *Lophophysema eversa* which encodes a sulfur oxidation pathway; [83] based on the Genome Taxonomy Database [84].

Based on the concatenated gene tree analyses, we further queried representative 16S rRNA gene sequences pulled from LS-SOB genome bins against the IMNGS 16S rRNA gene amplicon database [74], and placed the hits into the reference 16S rRNA gene tree using the Evolutionary Placement Algorithm [75]. As a result, 3 sets of short reads were placed into the branch leading to the dominant γ-proteobacterial symbiont sequences obtained from *I. basta* (Fig. S1). The closest two groups (I4, I6) comprised 5 (out of 6 total) reads derived from unspecified coral and sponge samples, 4 of which were reads from corals sampled from the same study site as *I. basta* for this study (Orpheus Island, Queensland, Australia). 141 reads were placed into the I7 group, of which 29 and 4 were derived from sponge and coral metagenomes, respectively (the other 112 reads were derived from other metagenomic data sets spanning a variety of environmental matrices). Most interestingly, out of this group, three reads were obtained from two sympatric marine sponge species (NE Atlantic) within the same genus, (*Hexadella dedritifera* and *Hexadella* cf. *dedritifera*) both of which are also affiliated with the same sponge family as *I. basta*, the Ianthellidae. These two closely related phylotypes, from *H. dedritifera* and *H*. cf. *detritifera*, respectively, exhibited 16S rRNA gene identities of ~97% (over 418 bp) with each other, 95-97% with the *I. basta* γ-symbiont, and were found to comprise 33-42% of the total amplicon dataset derived from these sponges [85]. Noting that these two Hexadella species harbor abundant and closely related γ-phylotypes, and also contain AOA-symbionts closely related to the AOA in *I. basta* [69], we assembled and binned two new γ-symbiont MAGs from the published raw read data set of these two Hexadella sponges.

The phylogenomic reconstruction confirmed that these two Hexadella γ-symbiont MAGs were most closely related to the *I. basta* γ-symbiont (Fig. 1), and AAI analyses indicated that the *I. basta* γ-symbiont shares AAI values of 76-80% with these two Hexadella γ-symbionts. Among the other LS-SOB genomes retrieved from marine sponges [35, 83, 86–88], the *I. basta* γ-symbiont shares AAI values of 54-59%. Since these identity values signify that the γ-symbiont represents a new species within a new genus along with the other two Hexadella γ-symbionts – 60-80% AAI is typical for organisms grouped at the genus level [89, 90] – we propose the name "*Candidatus* Taurinisymbion ianthellae". Taurinisymbion gen. nov. (Tau.ri.ni.sym'bi.on. N.L. n. taurinum, taurin; Gr. pref. sym, together; Gr. masc. part. n. bion, a living being; N.L. masc. n. Taurinisymbion, a taurin-degrading living partner) for the *I. basta* γ-symbiont. The name *Taurinisymbion* describes this organism's ability to utilize taurine as a source of energy and biomass whilst

residing in symbiosis within a sponge. The species name *ianthellae* refers to its discovery and description as a symbiont of the marine sponge, *I. basta*.

"Candidatus Taurisymbion ianthellae" is an abundant symbiont of Ianthella basta

Consistent with the high coverage of reads and peptides assigned to '*Ca*. Taurinisymbion ianthellae' in the metagenomic and metaproteomic data sets from *I. basta*, as well as the dominance of this phylotype in other *I. basta* studies [49–51], we observed a high abundance of this symbiont (Fig. 2) in the mesohyl of *I. basta* using fluorescence *in situ* hybridization (FISH) with a newly designed specific 16S rRNA-targeted probe. Quantitative FISH revealed that '*Ca*. Taurinisymbion ianthellae' accounted for 24 ± 5.6% (SD) of all cells hybridizing with the probe set EUB338-I-III targeting most bacteria (which does not cover the thaumarchaeal symbiont of *I. basta*). Moreover, absolute quantification of '*Ca*. Taurinisymbion ianthellae' using qPCR with newly designed symbiont specific primers showed an average absolute abundance of 2.78 ± 1.5 (SD) x 10^{10} 16S rRNA gene copies per g wet sponge, which is in the same range as the absolute abundances obtained for the dominant thaumarchaeal and alphaproteobacterial symbionts (Fig. S2). The ratio of '*Ca*. Taurinisymbion ianthellae' 16S rRNA sequences to the total 16S rRNA genes derived from qPCR assays (targeting the γ-, α-, and thaumarchaeal symbionts of *I. basta*) was 41.1 ± 34 (SD)%.

'Ca. Taurinisymbion ianthellae' expresses proteins for taurine catabolism and subsequent NH_4^+ and SO_4^{2-} export

To analyse the metabolic potential of '*Ca*. Taurinisymbion ianthellae' we annotated its MAG by employing the metaproteogenomic data set presented in [10] and were able to assign 149 proteins to this symbiont MAG. These proteins represented 35.7% in NSAF values of all proteins assigned to the *I. basta* microbiome (Table S2), highlighting the physiological dominance of '*Ca*. Taurinisymbion ianthellae'. From this metaproteogenomic dataset, we concluded that '*Ca*. Taurinisymbion ianthellae' is a facultative anaerobe with an ability to metabolize a variety of organic compounds. The genomic potential for the following major central metabolic pathways, such as glycolysis, the pentose phosphate pathway, the tricarboxylic acid (TCA) cycle, the glyoxylate bypass, a conventional respiratory chain (complex I -IV; two respiratory complex IV were found to be encoded, a cbb_3-

and a aa_3-type cytochrome c oxidase), complex V (Fig. 3, Table S3), as well as the genes for denitrification of NO_2^- to N_2O, and DMSP catabolism, were all present in the recovered MAG. A further discussion of a few of these genomic features, with a focus on DMSP metabolism is provided in the Supporting Information.

Most notably, '*Ca*. Taurinisymbion ianthellae' encodes a previously described pathway for taurine import and transamination [91]; *tauABC, tpa, xsc*] into sulfite via a desulfonated intermediate sulfoacetaldehyde, as well as the subsequent oxidation of the resultant toxic and highly reactive sulfite into sulfate via the cytoplasmic enzymes APS reductase (a*prAB*) and ATP sulfurylase (*sat*) [53]. This pathway consumes AMP and sulfite and releases ATP via substrate-level phosphorylation and sulfate and channels two electrons from the oxidation of sulfite with its very negative redox potential to the quinone pool via the membrane-bound QmoAB. Consistent with other sulfur oxidizing bacterial genomes the *qmoC* gene is replaced by *hdrBC* genes ([92] and references therein), with the *hdrBC* genes found to be adjacent to *qmoAB* in '*Ca*. Taurinisymbion ianthellae' and the HdrB subunit was expressed in the holobiont) (Fig. 3, Tables S2 & S3). For the potential export of sulfate, two putative sulfate permeases (COG0730 permease family, [93]; COG0659, sulP family permease), were detected in the '*Ca*. Taurinisymbion ianthellae' MAG. Interestingly, the gene encoding taurine dioxygenase (*tauD*), an alpha-ketoglutarate-dependent dioxygenase, which desulfonates taurine into aminoacetaldehyde (the fate of which is currently unknown) and sulfite, was also found encoded by '*Ca*. Taurinisymbion ianthellae'. TauD is involved in assimilation of sulfur from taurine in several aerobic bacteria [94].

Several of the genes involved in taurine degradation were also found to be expressed. Specifically, we detected the expression of the taurine transporter TauABC (with TauAB detected only when the 454 metagenome dataset was included), the two enzymes taurine-pyruvate aminotransferase (Tpa) and sulfoacetaldehyde acetyltransferase (Xsc) involved in the sequential dissimilation of taurine to sulfite via sulfoacetaldehyde, and two (Apr, Qmo) out of three proteins necessary (Sat was not detected in the metaproteome data set) for the subsequent oxidation of sulfite to sulfate. A phosphate acetyltransferase is present in the '*Ca*. Taurinisymbion ianthellae' MAG, which would convert the acetyl phosphate produced from the activity of Xsc (also producing sulfite) into acetyl-CoA for entry into the TCA as well as the glyoxylate bypass cycle. We detected the expression of the key enzymes malate dehydrogenase (Mdh) and isocitrate lyase (AceA), from each cycle, respectively, suggesting that the gyoxylate bypass is used for anabolic purposes while sulfite

oxidation is used for energy conservation by '*Ca*. Taurinisymbion ianthellae'. In addition to the expressed proteins in the pathway for taurine-derived sulfur and carbon compounds, we detected the expression of alanine dehydrogenase (Ald), which would replenish the pyruvate needed by the Tpa enzyme for taurine dissimilation as well as provide $NADH/H^+$ for respiration and NH_3 either for assimilation into glutamine by a highly expressed glutamine synthetase (GlnA) or transport out of the cell via an encoded ammonium transporter (*amtB* ; Fig. 3, Table S3), where it can be readily oxidized to nitrite, as previously demonstrated [10], by the dominant thaumarchaeal symbiont. While the expression of the taurine transporter has been observed in the γ-symbiont of *Olavius algarvensis* [95], the recent observations that marine sponge symbionts have the capacity for taurine utilization, is primarily based on gene presence [23, 24, 33–35], with the exception of metaproteomic evidence for *Ca*. Entotheonella phylotypes residing in the marine sponge *Theonella swinhoei* Y. However, this symbiont expressed multiple encoded copies of TauD-related proteins postulated to possibly function in the breakdown of small aromatic compounds [96].

Oxidation of sulfite to sulfate by taurine-degrading bacteria occurs via different pathways. Frequently periplasmic and cytoplasmic sulfite dehydrogenases are used [97, 98], but these enzymes were not detected in the '*Ca*. Taurinisymbion ianthellae' MAG. The two-step AMP-dependent indirect oxidation of sulfite to sulfate via APS in the cytoplasm employed by this symbiont, is infrequently detected in taurine degraders with examples found among the ubiquitous, pelagic SAR11 ([53]; but most SAR11 lack ATP sulfurylase), the γ-3 symbiont in the gutless oligochaete, *Olavius algarvensis* [99], and two marine sponge symbionts [23, 24]. Although a metaproteomic study in Antarctic waters has previously revealed the expression in SAR11-associated peptides of this particular pathway for taurine dissimilation (Tpa, Xsc) followed by sulfite oxidation (AprAB) [53], SAR11 in culture has not yet been shown to excrete sulfate in the presence of taurine [100, 101], or other forms of reduced sulfur such as DMSP and methionine, perhaps owing to its dependence on organic sources of sulfur for assimilation rather than seawater sulfate [102].

Taurine metabolism in the Ianthella basta holobiont

Based on the findings of the metaproteogenomic data set, we investigated taurine metabolism in the *I. basta* holobiont experimentally. Firstly, NMR and LCMS analyses of the 90% MeOH extract and the aqueous Fr 1 confirmed that taurine was present in this sponge (^{1}H NMR diagnostic triplet signals: δ_H 3.26 [t, 2H, 6.6 Hz] and δ_H 3.42 [t, 2H, J = 6.6 Hz, Fig. 4a); LCMS Rt = 2.8 mins and $[M+H]^+$ 126.4 *m/z* with isotope distribution indicative of sulfur; LCMS^2 $[M+H-H_2O]^+$ 108.4 *m/z* Fig. 4a, Fig. S3)[103]. The natural concentration of taurine, determined by qNMR, was 5.48 ± 0.69 µmol g^{-1} wet wt., which is in the mid-range of previously reported values for six other marine sponges [104]. HPLC analysis at t_0 (1 mM taurine added), t_{12} and t_{48} (additional 0.6 mM taurine pulse at t_{36}) confirmed uptake of taurine by the *I. basta* holobiont (1.20 ± 0.05 mM taurine in seawater as compared to control incubations 1.73 ± 0.02 mM taurine in seawater, Kruskal-Wallis $p < 0.05$, Fig. S4). Subsequently, whole sponge and total nucleic acids elemental analyzer isotope ratio mass spectrometry (EA-IRMS) analyses of *I. basta* sponge clones that underwent additions of an equimolar mixture of ^{13}C- and ^{15}N-labeled taurine in 48 h incubations showed enrichment in ^{13}C and ^{15}N relative to control sponge clones (Fig. 4b, Fig. S5). While it cannot be excluded that sorption of labeled taurine contributed to the isotopic enrichment in the whole sponge experiments, the detection of labeled total nucleic acids clearly indicated assimilation and incorporation of labelled taurine into *I. basta* holobiont biomass. Moreover, NanoSIMS analyses combined with fluorescence microscopy via DAPI staining conducted on dissociated sponge extracellular material revealed accumulation of taurine-derived C and N within regions that were similar in size and shape to typical sponge microbial symbiont cells previously visualized in *I. basta* by transmission electron microscopy [50]. The isotope label content of these cells ranged from 0.42 – 1.15 at% ^{15}N and 1.09 – 1.47 at% ^{13}C (Fig. 4, Fig. S6) which significantly exceeded the values determined within regions of the sponge extracellular matrix (Mann–Whitney U-test, $p < 0.001$), consistent with (a) population(s) of microorganisms specialized in using taurine (Fig. S7). Unfortunately, the sponge samples (three clones from the same sponge individual of which two were used for NanoSIMS analyses) from the taurine incubation experiments could not be analyzed by combining fluorescence *in situ* hybridization (FISH) with symbiont specific probes and NanoSIMS as this sponge individual exhibited very high autofluorescence at each wavelength typically exploited for the detection of FISH-probe derived signals.

From the whole sponge EA-IRMS data, we were able to estimate uptake rates of taurine-derived C and N assimilated into whole *I. basta* holobiont biomass and obtained values of 1.38 ± 0.3 nmol C min^{-1} g^{-1} sponge wet wt (± SE) and 0.74 ± 0.2 nmol N min^{-1} g^{-1} sponge wet wt (± SE). These *I. basta* holobiont taurine-derived carbon uptake rates correspond to approximately 4 – 10% of the bulk DOC uptake rates reported for the more diverse microbiome of the marine sponge *Aplysina aerophoba* [105]. The C/N ratio of the assimilated taurine by the *I. basta* holobiont was 1.86 ± 0.09 (SD) and 2.37 ± 0.03 (SD), for the whole sponge and nucleic acids-based analyses, respectively which were lower than the corresponding total C/N ratios of 4.6 ± 0.07 (SD) and 3.21 ± 0.2 (SD) determined in the same sponges, as well as those found for sponge clones that were not incubated with isotope-labeled taurine (4.6 ± 0.15 and 3.40 ± 0.03). These values indicate that the holobiont assimilated the taurine-derived nitrogen more efficiently than the corresponding carbon, which is consistent with the inherent C/N stoichiometry of taurine (i.e., 2.0). An extended discussion regarding the fractions of taurine-derived C and N incorporated into whole *I. basta* holobiont biomass is provided in the Supplementary Information.

Taurine catabolism by Ianthella basta holobiont results in the accumulation of inorganic S and N species

Some microbial pure cultures catabolizing taurine oxidize sulfite, obtained via cleavage from the sulfonate moiety, to sulfate which is subsequently excreted [106–108]. Considering that metaproteogenomic analyses predicted sulfate as a secreted end product of '*Ca*. Taurinisymbion ianthellae' taurine metabolism, we analyzed whether the *I. basta* holobiont produced sulfate (SO_4^{2-}) in experiments with and without added taurine. Specifically, 48 h incubations of *I. basta* clones amended with (in total 1.6 mM) and without taurine were performed in sulfate-free artificial seawater (SFASW). SFASW was used in these incubations to facilitate detection of sulfate formation by the holobiont. Pairwise comparisons in incubations with sponges in SFASW without the addition of taurine, resulted in a small but significant production of SO_4^{2-} after 12 h indicating *in vivo* production of SO_4^{2-} ($p < 0.05$, one-tailed t-test) (Fig. 5a). In incubations with *I. basta* clones and taurine, a similarly small increase was seen at 12 h ($p < 0.05$, one-tailed t-test), with SO_4^{2-} production strongly increasing between the 12 h and 48 h time points, indicating a metabolic lag effect (Fig. 5a), with final SO_4^{2-} concentrations of 590 ± 89 (SE) µM SO_4^{2-} (59.0 ± 2.0 µmol g^{-1} wet wt) that were significantly higher than the SO_4^{2-}

concentrations at t = 0 and t = 12 h (one-way ANOVA followed by Holm-Sidak tests, $p < 0.001$) and also significantly higher than all control incubations including the incubations with sponge clones but without taurine at t = 48 h (one-way ANOVA followed by Holm-Sidak pairwise multiple comparison tests, $p < 0.001$). Two additional incubation experiments, with refined temporal resolution (t = 0, 12, 24, 36 and 48 h) using 1 mM and 100 µM unlabeled taurine amendments, respectively, resembled the results of the previous experiment and displayed a significant SO_4^{2-} increase after 48 h for both taurine treatments (one-way ANOVA followed by Tukey pairwise multiple comparison tests, $p < 0.05$) with essentially a full recovery of the +100 µM taurine sulfonate in the form of sulfate$^-$ after 48h (Fig. S9).

Moreover, we observed NH_4^+ and NO_2^- production in *I. basta* incubations, with and without added unlabeled taurine, where NH_4^+ production at the end of the experiment with added taurine, drastically exceeded those of *I. basta* incubations without added taurine consistent with the production of ammonium from taurine (Fig. 5a; two-tailed t-test, $p < 0.05$). Furthermore, a clear increase in NO_2^- production occurred within the first 12 h and which was significant for incubations with added taurine (Fig. 5a, one-way ANOVA followed by Tukey pairwise multiple comparison tests, $p < 0.05$). NH_4^+ and NO_2^- production in *I. basta* has previously been observed [10] and the NO_2^- production was attributed to the only ammonia-oxidizing symbiont, '*Ca*. Nitrosospongia ianthellae'. At the end of the experiment, NO_2^- concentrations decreased in the incubations with added taurine, consistent with the previously demonstrated inhibition of ammonia oxidation at concentrations ≥100 µM NH_4^+ in the *I.* basta holobiont and/or with the concomitant increased hypoxia facilitating denitrification activities [10]. Additional experiments with refined temporal resolution, displayed the same general trends (Fig. S9).

Another experiment was carried out in the presence of only 100 µM NH_4^+ to evaluate whether high NH_4^+ concentrations could inhibit SO_4^{2-} production by the *I. basta* holobiont (SOM Methods). Results indicated that SO_4^{2-} production was not significantly affected (one-way ANOVA, $p > 0.1$: for t = 12 and t =48 h) relative to the controls containing sponges in SFASW without added taurine (Figure S10).

In addition, FSW incubations of the *I. basta* holobiont with ^{15}N-labeled taurine were performed. In these experiments, we were able to detect $^{15}NH_4^+$ and $^{15}NO_2^-$ formation by *I. basta* sponge clones (Fig. 5b),

demonstrating taurine metabolism and oxidation of taurine-derived ammonia to nitrite by the sponge holobiont. Importantly, the amount of $^{15}NH_4^+$ and $^{15}NO_2^-$ derived from ^{15}N-labeled taurine in incubations with *I. basta* was always higher than the amount detected in FSW control incubations without *I. basta* at t = 12 and t = 48 h (Figure 5b; one-way ANOVA followed by Student-Newman-Keuls pairwise multiple comparison tests, $p < 0.05$; $^{15}NO_2^-$ in FSW control incubations were undetectable in all samples). This demonstrates that these successive conversions were catalyzed by holobiont members and that this process starts as early as 12 h, suggesting that the similarly observed increase in SO_4^{2-} was also derived from taurine. When looking at bulk NH_4^+ and NO_2^- concentrations in these FSW incubations, the amount of both compounds produced with only *I. basta* clones without externally added taurine still greatly exceeded those FSW incubations without sponge clones and added taurine providing additional support for the production of these compounds by *I. basta* holobiont members.

Recently, several laboratory and field-based studies have documented the exchange of sulfonates between marine bacteria and eukaryotic phytoplankton, with taurine (or its derivatives), always being one of the main sulfonates involved [30–32]. In co-culture, the coastal diatom *Pseudo-nitzschia multiseries* apparently provides a *Sulfitobacter* strain (SA11) with taurine in exchange for the plant hormone indole-3-acetic acid as well as ammonium [109]. Similarly, cross-feeding between marine nitrite oxidizers and ammonia oxidizers has been demonstrated wherein urea or cyanate is first processed by nitrite oxidizers [110, 111], thereby providing the cleaved ammonia for oxidation to nitrite. While marine Thaumarchaeota have been shown to directly utilize urea and cyanate [112] as well as taurine exuded by mesozooplankton [113], the mechanisms for the direct utilization of these dissolved organic compounds has yet to be elucidated and indirect utilization remains a confounding factor.

A proposed model of an auxotrophy network between symbionts and the sponge host

In the *I. basta* metagenome we found no indications for taurine biosynthesis by its microbial symbionts. Consequently, it is most parsimonious that taurine detected in the *I. basta* holobiont is synthesized by the sponge and after release, via export or sponge cell lysis, utilized by '*Ca*. Taurinisymbion ianthellae'. Taurine biosynthesis pathways in mammalian and invertebrate tissues use cysteine as a precursor [40] and references

621 therein] and cysteine synthesis in metazoans requires methionine [114]. The methionine synthesis pathway,
622 along with the biosynthesis pathways for several other essential amino acids, are generally lacking in metazoans
623 [115, 116], and thus these compounds are typically acquired via heterotrophy. While at least some sponges seem
624 to possess the genomic repertoire for cysteine and methionine synthesis [117], so far, no studies have confirmed
625 their biosynthesis in radiolabeled amino acid precursor or feeding studies whereas five species of scleratinian
626 corals can produce low amounts of methionine but not cysteine [118]. '*Ca*. Taurinisymbion ianthellae' encodes
627 pathways for the synthesis of methionine and cysteine (Fig. S11) which are connected with the degradation of
628 taurine and DMSP (Fig. 3) and also encodes several copies of EamA domain-containing proteins (IPR000620)
629 and two copies of LeuE-type export proteins (IPR001123) (Fig. 3 & Table S5), with both families containing
630 homologous representatives demonstrated to export cysteine [119] and methionine [120], respectively. Thus, it is
631 tempting to speculate that this symbiont synthesizes and exports methionine and cysteine which is then taken up
632 and metabolized by *I. basta* and the latter is used as a precursor for taurine biosynthesis. Although the
633 methionine synthase (MetH)-containing pathway for methionine biosynthesis in '*Ca*. Taurinisymbion ianthellae'
634 is vitamin B_{12} dependent (this organism also encodes a vitamin B_{12}-independent pathway using DMSP as
635 precursor as well as the cobalamin-independent methionine synthase, MetE; Fig 3, Fig S11), its MAG does not
636 contain the genes required for synthesis of this vitamin while encoding a putative vitamin B_{12} transporter
637 BtuCDF (Fig. 3 & Table S5). As the thaumarchaeal symbiont of *I. basta* '*Ca.* Nitrosospongia ianthellae' has the
638 genomic repertoire for cobalamin (vitamin B_{12}) biosynthesis [10] it is conceivable that it provides vitamin B_{12}
639 for methionine biosynthesis in '*Ca*. Taurinisymbion ianthellae' if DMSP is not available, while receiving
640 ammonia produced by the γ-symbiont from taurine degradation. Nitrite formed by ammonia oxidation by '*Ca.*
641 Nitrosospongia ianthellae' can then serve under low oxygen concentrations as electron acceptor in '*Ca*.
642 Taurinisymbion ianthellae'. Furthermore, since nitric oxide has been shown to have an immediate contractile
643 effect on sponges [121] and seems to be an ancient and key regulator in the marine sponge life cycle [122], the
644 fact that '*Ca*. Taurinisymbion ianthellae' encodes two denitrification genes – a nitrite reductase, *nirK* and a
645 single subunit quinol-dependent nitric oxide reductase, *qNOR* [123] – that produces and consumes NO, suggests
646 that this symbiont may be able to modulate host behavior. The frequent presence of an incomplete denitrification
647 pathway along with the quinol-dependent *qNOR* – a nitrite reductase commonly found in pathogenic species

[124] – in other sponge metagenomes [26], further points at the possibility that this is a widespread feature of microbial symbionts residing in marine sponges. Taken together, our data indicate a tightly connected metabolic network in the *I. basta* holobiont (Fig. 6), albeit in contrast to selected other sponges no data are yet available for *I. basta* on the uptake of amino acids directly from the environment [105, 125] and on the acquisition of amino acids from ingested free-living and symbiotic prokaryotes [126].

Conclusions

In this study, we showed through a combination of metaproteogenomic analyses and incubation experiments combined with isotope labeling, that the dominant *I. basta* gammaproteobacterial symbiont '*Ca.* Taurinisymbion ianthellae' uses endogenously occurring taurine within the sponge holobiont for assimilation and energy conservation. We experimentally demonstrated that the taurine dissimilation products sulfate and ammonia are secreted and that the latter compound is used for ammonia oxidation by the dominant thaumarchaeal symbiont – '*Ca.* Nitrosospongia ianthellae'. Taurine seems to be an important metabolite not only in *I. basta* but in many sponge holobiont systems as indicated by the seeming ubiquity of taurine and taurine dissimilating genes within sponge microbiomes [23, 24, 33–35], with the appearance of a specific taurine-dissimilation/sulfite-oxidation pathway restricted mostly to symbiotic microorganisms [23, 24, 99]. Taurine also appears to be a central metabolite in several other prominent marine invertebrate symbioses such as in cnidarians and various bivalve species [39, 40, 127, 128]. Future research is needed to further disentangle the mechanisms of taurine synthesis via symbiont-derived or environmentally supplied precursors in these holobionts, to better understand the role of exogenous taurine uptake, and the numerous roles taurine may play for the functioning of these symbioses.

Acknowledgements

We thank Emmanuelle Botte for assisting with experimental incubations, Heidi Luter for assisting with field collections and Bettina Glasl and Pam Engelberts for helpful discussions. Florian Moeller and Maria

Mooshammer were supported by the ERC Advanced Grant Nitricare (294343 to MW). We thank Bernhard Schink for valuable advice regarding the provisional naming of the gammaproteobacterial symbiont.

References

1. Bell JJ. The functional roles of marine sponges. *Estuarine, Coastal and Shelf Science* 2008; **79**: 341–353.
2. de Goeij J, van den Berg H, van Oostveen M, Epping E, van Duyl F. Major bulk dissolved organic carbon (DOC) removal by encrusting coral reef cavity sponges. *Mar Ecol Prog Ser* 2008; **357**: 139–151.
3. de Goeij JM, van Oevelen D, Vermeij MJA, Osinga R, Middelburg JJ, de Goeij AFPM, et al. Surviving in a Marine Desert: The Sponge Loop Retains Resources Within Coral Reefs. *Science* 2013; **342**: 108–110.
4. Rix L, de Goeij JM, Mueller CE, Struck U, Middelburg JJ, van Duyl FC, et al. Coral mucus fuels the sponge loop in warm- and cold-water coral reef ecosystems. *Scientific Reports* 2016; **6**: 18715.
5. Webster NS, Thomas T. The Sponge Hologenome. *mBio* 2016; **7**.
6. Zhang F, Jonas L, Lin H, Hill RT. Microbially mediated nutrient cycles in marine sponges. *FEMS Microbiol Ecol* 2019; **95**.
7. Wilkinson CR. Net Primary Productivity in Coral Reef Sponges. *Science* 1983; **219**: 410–412.
8. Wilkinson CR, Fay P. Nitrogen fixation in coral reef sponges with symbiotic cyanobacteria. *Nature* 1979; **279**: 527–529.
9. Bayer K, Schmitt S, Hentschel U. Physiology, phylogeny and *in situ* evidence for bacterial and archaeal nitrifiers in the marine sponge *Aplysina aerophoba*. *Environmental Microbiology* 2008; **10**: 2942–2955.
10. Moeller FU, Webster NS, Herbold CW, Behnam F, Domman D, Albertsen M, et al. Characterization of a thaumarchaeal symbiont that drives incomplete nitrification in the tropical sponge Ianthella basta. *Environmental Microbiology* 2019; **21**: 3831–3854.
11. Hoffmann F, Larsen O, Thiel V, Rapp HT, Pape T, Michaelis W, et al. An Anaerobic World in Sponges. *Geomicrobiology Journal* 2005; **22**: 1–10.
12. Hoffmann F, Radax R, Woebken D, Holtappels M, Lavik G, Rapp HT, et al. Complex nitrogen cycling in the sponge *Geodia barretti*. *Environmental Microbiology* 2009; **11**: 2228–2243.
13. Freeman CJ, Thacker RW. Complex interactions between marine sponges and their symbiotic microbial communities. *Limnology and Oceanography* 2011; **56**: 1577–1586.
14. Freeman CJ, Thacker RW, Baker DM, Fogel ML. Quality or quantity: is nutrient transfer driven more by symbiont identity and productivity than by symbiont abundance? *The ISME Journal* 2013; **7**: 1116–1125.
15. Hudspith M, Rix L, Achlatis M, Bougoure J, Guagliardo P, Clode PL, et al. Subcellular view of host–microbiome nutrient exchange in sponges: insights into the ecological success of an early metazoan–microbe symbiosis. *Microbiome* 2021; **9**: 44.
16. Taylor MW, Radax R, Steger D, Wagner M. Sponge-associated microorganisms: evolution, ecology, and biotechnological potential. *Microbiol Mol Biol Rev* 2007; **71**: 295–347.
17. Webster NS, Taylor MW. Marine sponges and their microbial symbionts: love and other relationships: Marine sponge microbiology. *Environmental Microbiology* 2012; **14**: 335–346.
18. Thomas T, Moitinho-Silva L, Lurgi M, Björk JR, Easson C, Astudillo-García C, et al. Diversity, structure and convergent evolution of the global sponge microbiome. *Nature Communications* 2016; **7**.

19. Siegl A, Kamke J, Hochmuth T, Piel J, Richter M, Liang C, et al. Single-cell genomics reveals the lifestyle of Poribacteria, a candidate phylum symbiotically associated with marine sponges. *The ISME Journal* 2011; **5**: 61–70.

20. Moitinho-Silva L, Díez-Vives C, Batani G, Esteves AI, Jahn MT, Thomas T. Integrated metabolism in sponge–microbe symbiosis revealed by genome-centered metatranscriptomics. *The ISME Journal* 2017; **11**: 1651–1666.

21. Fiore CL, Labrie M, Jarett JK, Lesser MP. Transcriptional activity of the giant barrel sponge, Xestospongia muta Holobiont: molecular evidence for metabolic interchange. *Frontiers in Microbiology* 2015; **6**.

22. Moreno-Pino M, Cristi A, Gillooly JF, Trefault N. Characterizing the microbiomes of Antarctic sponges: a functional metagenomic approach. *Scientific Reports* 2020; **10**: 645.

23. Tian R-M, Wang Y, Bougouffa S, Gao Z-M, Cai L, Bajic V, et al. Genomic analysis reveals versatile heterotrophic capacity of a potentially symbiotic sulfur-oxidizing bacterium in sponge: A versatile SOB as a potential sponge symbiont. *Environmental Microbiology* 2014; **16**: 3548–3561.

24. Gauthier M-EA, Watson JR, Degnan SM. Draft Genomes Shed Light on the Dual Bacterial Symbiosis that Dominates the Microbiome of the Coral Reef Sponge Amphimedon queenslandica. *Frontiers in Marine Science* 2016; **3**.

25. Hallam SJ, Konstantinidis KT, Putnam N, Schleper C, Watanabe Y -i., Sugahara J, et al. Genomic analysis of the uncultivated marine crenarchaeote Cenarchaeum symbiosum. *Proceedings of the National Academy of Sciences* 2006; **103**: 18296–18301.

26. Fan L, Reynolds D, Liu M, Stark M, Kjelleberg S, Webster NS, et al. Functional equivalence and evolutionary convergence in complex communities of microbial sponge symbionts. *Proceedings of the National Academy of Sciences* 2012; **109**: E1878–E1887.

27. Hentschel U, Piel J, Degnan SM, Taylor MW. Genomic insights into the marine sponge microbiome. *Nature Reviews Microbiology* 2012; **10**: 641–654.

28. Liu M, Fan L, Zhong L, Kjelleberg S, Thomas T. Metaproteogenomic analysis of a community of sponge symbionts. *The ISME Journal* 2012; **6**: 1515–1525.

29. Hooper JNA, Capon RJ, Keenan CP, Parry DL, Smit N. Chemotaxonomy of marine sponges: Families Microcionidae, Raspailiidae and Axinellidae, and their relationships with other families in the orders Poecilosclerida and Axinellida (Porifera : Demospongiae). *Invert Systematics* 1992; **6**: 261–301.

30. Durham BP, Sharma S, Luo H, Smith CB, Amin SA, Bender SJ, et al. Cryptic carbon and sulfur cycling between surface ocean plankton. *Proc Natl Acad Sci USA* 2015; **112**: 453–457.

31. Landa M, Burns AS, Roth SJ, Moran MA. Bacterial transcriptome remodeling during sequential co-culture with a marine dinoflagellate and diatom. *ISME J* 2017; **11**: 2677–2690.

32. Durham BP, Boysen AK, Carlson LT, Groussman RD, Heal KR, Cain KR, et al. Sulfonate-based networks between eukaryotic phytoplankton and heterotrophic bacteria in the surface ocean. *Nat Microbiol* 2019; **4**: 1706–1715.

33. Karimi E, Keller-Costa T, Slaby BM, Cox CJ, da Rocha UN, Hentschel U, et al. Genomic blueprints of sponge-prokaryote symbiosis are shared by low abundant and cultivatable Alphaproteobacteria. *Scientific Reports* 2019; **9**: 1999.

34. Botté ES, Nielsen S, Abdul Wahab MA, Webster J, Robbins S, Thomas T, et al. Changes in the metabolic potential of the sponge microbiome under ocean acidification. *Nature Communications* 2019; **10**: 4134.

35. Engelberts JP, Robbins SJ, de Goeij JM, Aranda M, Bell SC, Webster NS. Characterization of a sponge microbiome using an integrative genome-centric approach. *The ISME Journal* 2020; **14**: 1100–1110.

36. Atlas M, Bahl JJ, Roeske W, Bressler R. In vitro osmoregulation of taurine in fetal mouse hearts. *Journal of Molecular and Cellular Cardiology* 1984; **16**: 311–320.

37. Schaffer S, Takahashi K, Azuma J. Role of osmoregulation in the actions of taurine. *Amino Acids* 2000; **19**: 527–546.

38. Huxtable RJ. Physiological actions of taurine. *Physiological Reviews* 1992; **72**: 101–163.

39. Lee R, Childress J, Desaulniers N. The effects of exposure to ammonia on ammonia and taurine pools of the symbiotic clam. *Journal of Experimental Biology* 1997; **200**: 2797–2805.

40. Joyner JL, Peyer SM, Lee RW. Possible Roles of Sulfur-Containing Amino Acids in a Chemoautotrophic Bacterium-Mollusc Symbiosis. *The Biological Bulletin* 2003; **205**: 331–338.

41. Alberic P, Boulegue J. Unusual amino compounds in the tissues of Calyptogena phaseoliformis (Japan Trench): Possible link to symbiosis. *Progress in Oceanography* 1990; **24**: 89–101.

42. Conway NM, Howes BL, McDowell Capuzzo JE, Turner RD, Cavanaugh CM. Characterization and site description of Solemya borealis (Bivalvia; Solemyidae), another bivalve-bacteria symbiosis. *Marine Biology* 1992; **112**: 601–613.

43. Conway NM, McDowell Capuzzo JE. High taurine levels in the Solemya velum symbiosis. *Comparative Biochemistry and Physiology Part B: Comparative Biochemistry* 1992; **102**: 175–185.

44. Pranal V, Fiala-Médioni A, Colomines J. Amino acid and related compound composition in two symbiotic mytilid species from hydrothermal vents. *Mar Ecol Prog Ser* 1995; **119**: 155–166.

45. Pruski AM, Fiala-Médioni, A., Boulegue, J., Colomines, J.C. Sulphur metabolism in chemosynthetic symbiont-containing invertebrates from hydrothermal vents. *Cahiers de Biologie Marine* 1997; **2**.

46. Pallas PS. Elenchus zoophytorum sistens generum adumbrationes generaliores et specierum cognitarum succintas descriptiones, cum selectis auctorum synonymis / P. S. Pallas. 1766. Apud Petrum van Cleef, Hagae-Comitum :

47. Bergquist PR, Kelly-Borges M. Systematics and Biogeography of the Genus Ianthella (Demospongiae: Verongida: Ianthellidae) in the south-west Pacific. *Beagle: Records of the Museums and Art Galleries of the Northern Territory, The* 1995; **12**: 151.

48. Hentschel U, Usher KM, Taylor MW. Marine sponges as microbial fermenters: Marine sponges as microbial fermenters. *FEMS Microbiology Ecology* 2006; **55**: 167–177.

49. Webster NS, Taylor MW, Behnam F, Lücker S, Rattei T, Whalan S, et al. Deep sequencing reveals exceptional diversity and modes of transmission for bacterial sponge symbionts. *Environmental Microbiology* 2009.

50. Luter HM, Whalan S, Webster NS. Exploring the Role of Microorganisms in the Disease-Like Syndrome Affecting the Sponge Ianthella basta. *Applied and Environmental Microbiology* 2010; **76**: 5736–5744.

51. Freckelton ML, Luter HM, Andreakis N, Webster NS, Motti CA. Qualitative variation in colour morphotypes of Ianthella basta (Porifera: Verongida). *Hydrobiologia* 2012; **687**: 191–203.

52. Luter HM, Whalan S, Webster NS. Thermal and Sedimentation Stress Are Unlikely Causes of Brown Spot Syndrome in the Coral Reef Sponge, Ianthella basta. *PLoS ONE* 2012; **7**: e39779.

53. Williams TJ, Long E, Evans F, DeMaere MZ, Lauro FM, Raftery MJ, et al. A metaproteomic assessment of winter and summer bacterioplankton from Antarctic Peninsula coastal surface waters. *The ISME Journal* 2012; **6**: 1883–1900.

54. Lu X, Zou L, Clevinger C, Liu Q, Hollibaugh JT, Mou X. Temporal dynamics and depth variations of dissolved free amino acids and polyamines in coastal seawater determined by high-performance liquid chromatography. *Marine Chemistry* 2014; **163**: 36–44.

55. Stoecker K, Dorninger C, Daims H, Wagner M. Double Labeling of Oligonucleotide Probes for Fluorescence In Situ Hybridization (DOPE-FISH) Improves Signal Intensity and Increases rRNA Accessibility. *Applied and Environmental Microbiology* 2010; **76**: 922–926.

56. Daims H, Brühl A, Amann R, Schleifer K-H, Wagner M. The Domain-specific Probe EUB338 is Insufficient for the Detection of all Bacteria: Development and Evaluation of a more Comprehensive Probe Set. *Systematic and Applied Microbiology* 1999; **22**: 434–444.

57. Wallner G, Amann R, Beisker W. Optimizing fluorescent in situ hybridization with rRNA-targeted oligonucleotide probes for flow cytometric identification of microorganisms. *Cytometry* 1993; **14**: 136–143.

58. Tapiolas DM, Raina J-B, Lutz A, Willis BL, Motti CA. Direct measurement of dimethylsulfoniopropionate (DMSP) in reef-building corals using quantitative nuclear magnetic resonance (qNMR) spectroscopy. *Journal of Experimental Marine Biology and Ecology* 2013; **443**: 85–89.

59. Angel R, Claus P, Conrad R. Methanogenic archaea are globally ubiquitous in aerated soils and become active under wet anoxic conditions. *ISME J* 2012; **6**: 847–862.

60. Sørensen P, Jensen ES. Sequential diffusion of ammonium and nitrate from soil extracts to a polytetrafluoroethylene trap for 15N determination. *Analytica Chimica Acta* 1991; **252**: 201–203.

61. Lachouani P, Frank AH, Wanek W. A suite of sensitive chemical methods to determine the δ15N of ammonium, nitrate and total dissolved N in soil extracts. *Rapid Communications in Mass Spectrometry* 2010; **24**: 3615–3623.

62. Poczatek C, Kaufman Z, Lechene C. OpenMIMS ImageJ Plugin Guide Opening MIMS images. 2009. Harvard Med. Sch.

63. Schindelin J, Arganda-Carreras I, Frise E, Kaynig V, Longair M, Pietzsch T, et al. Fiji: an open-source platform for biological-image analysis. *Nat Methods* 2012; **9**: 676–682.

64. Bankevich A, Nurk S, Antipov D, Gurevich AA, Dvorkin M, Kulikov AS, et al. SPAdes: A New Genome Assembly Algorithm and Its Applications to Single-Cell Sequencing. *Journal of Computational Biology* 2012; **19**: 455–477.

65. Kang DD, Froula J, Egan R, Wang Z. MetaBAT, an efficient tool for accurately reconstructing single genomes from complex microbial communities. *PeerJ* 2015; **3**: e1165.

66. Olm MR, Brown CT, Brooks B, Banfield JF. dRep: a tool for fast and accurate genomic comparisons that enables improved genome recovery from metagenomes through de-replication. *The ISME Journal* 2017; **11**: 2864–2868.

67. Parks DH, Imelfort M, Skennerton CT, Hugenholtz P, Tyson GW. CheckM: assessing the quality of microbial genomes recovered from isolates, single cells, and metagenomes. *Genome Research* 2015; **25**: 1043–1055.

68. Vallenet D, Engelen S, Mornico D, Cruveiller S, Fleury L, Lajus A, et al. MicroScope: a platform for microbial genome annotation and comparative genomics. *Database* 2009; **2009**.

69. Zhang S, Song W, Wemheuer B, Reveillaud J, Webster N, Thomas T. Comparative Genomics Reveals Ecological and Evolutionary Insights into Sponge-Associated *Thaumarchaeota*. *mSystems* 2019; **4**: e00288-19.

70. Simister RL, Deines P, Botté ES, Webster NS, Taylor MW. Sponge-specific clusters revisited: a comprehensive phylogeny of sponge-associated microorganisms: Sponge-associated microorganisms. *Environmental Microbiology* 2012; **14**: 517–524.

71. Nguyen L-T, Schmidt HA, von Haeseler A, Minh BQ. IQ-TREE: A Fast and Effective Stochastic Algorithm for Estimating Maximum-Likelihood Phylogenies. *Molecular Biology and Evolution* 2015; **32**: 268–274.

72. Kalyaanamoorthy S, Minh BQ, Wong TKF, von Haeseler A, Jermiin LS. ModelFinder: fast model selection for accurate phylogenetic estimates. *Nature Methods* 2017; **14**: 587–589.

73. Hoang DT, Chernomor O, von Haeseler A, Minh BQ, Vinh LS. UFBoot2: Improving the Ultrafast Bootstrap Approximation. *Molecular Biology and Evolution* 2018; **35**: 518–522.

74. Lagkouvardos I, Joseph D, Kapfhammer M, Giritli S, Horn M, Haller D, et al. IMNGS: A comprehensive open resource of processed 16S rRNA microbial profiles for ecology and diversity studies. *Scientific Reports* 2016; **6**.

75. Berger SA, Krompass D, Stamatakis A. Performance, Accuracy, and Web Server for Evolutionary Placement of Short Sequence Reads under Maximum Likelihood. *Systematic Biology* 2011; **60**: 291–302.

76. Stamatakis A. RAxML version 8: a tool for phylogenetic analysis and post-analysis of large phylogenies. *Bioinformatics* 2014; **30**: 1312–1313.

77. Otto A, Bernhardt J, Meyer H, Schaffer M, Herbst F-A, Siebourg J, et al. Systems-wide temporal proteomic profiling in glucose-starved Bacillus subtilis. *Nature Communications* 2010; **1**: 137.

78. Verberkmoes NC, Russell AL, Shah M, Godzik A, Rosenquist M, Halfvarson J, et al. Shotgun metaproteomics of the human distal gut microbiota. *The ISME Journal* 2009; **3**: 179–189.

79. Heinz E, Williams TA, Nakjang S, Noël CJ, Swan DC, Goldberg AV, et al. The Genome of the Obligate Intracellular Parasite Trachipleistophora hominis: New Insights into Microsporidian Genome Dynamics and Reductive Evolution. *PLoS Pathogens* 2012; **8**: e1002979.

80. Peng J, Elias JE, Thoreen CC, Licklider LJ, Gygi SP. Evaluation of Multidimensional Chromatography Coupled with Tandem Mass Spectrometry (LC/LC−MS/MS) for Large-Scale Protein Analysis: The Yeast Proteome. *Journal of Proteome Research* 2003; **2**: 43–50.

81. Elias JE, Gygi SP. Target-decoy search strategy for increased confidence in large-scale protein identifications by mass spectrometry. *Nature Methods* 2007; **4**: 207–214.

82. Florens L, Carozza M, Swanson S, Fournier M, Coleman M, Workman J, et al. Analyzing chromatin remodeling complexes using shotgun proteomics and normalized spectral abundance factors. *Methods* 2006; **40**: 303–311.

83. Tian R-M, Sun J, Cai L, Zhang W-P, Zhou G-W, Qiu J-W, et al. The deep-sea glass sponge *L ophophysema eversa* harbours potential symbionts responsible for the nutrient conversions of carbon, nitrogen and sulfur: Potential symbionts in a glass sponge. *Environmental Microbiology* 2016; **18**: 2481–2494.

84. Parks DH, Chuvochina M, Waite DW, Rinke C, Skarshewski A, Chaumeil P-A, et al. A standardized bacterial taxonomy based on genome phylogeny substantially revises the tree of life. *Nature Biotechnology* 2018.

85. Reveillaud J, Maignien L, Eren AM, Huber JA, Apprill A, Sogin ML, et al. Host-specificity among abundant and rare taxa in the sponge microbiome. *The ISME Journal* 2014; **8**: 1198–1209.

86. Rust M, Helfrich EJN, Freeman MF, Nanudorn P, Field CM, Rückert C, et al. A multiproducer microbiome generates chemical diversity in the marine sponge *Mycale hentscheli*. *Proc Natl Acad Sci USA* 2020; **117**: 9508–9518.

87. Storey MA, Andreassend SK, Bracegirdle J, Brown A, Keyzers RA, Ackerley DF, et al. Metagenomic Exploration of the Marine Sponge *Mycale hentscheli* Uncovers Multiple Polyketide-Producing Bacterial Symbionts. *mBio* 2020; **11**: e02997-19.

88. Glasl B, Robbins S, Frade PR, Marangon E, Laffy PW, Bourne DG, et al. Comparative genome-centric analysis reveals seasonal variation in the function of coral reef microbiomes. *ISME J* 2020; **14**: 1435–1450.

89. Luo C, Rodriguez-R LM, Konstantinidis KT. MyTaxa: an advanced taxonomic classifier for genomic and metagenomic sequences. *Nucleic Acids Research* 2014; **42**: e73–e73.

90. Konstantinidis KT, Rosselló-Móra R, Amann R. Uncultivated microbes in need of their own taxonomy. *The ISME Journal* 2017; **11**: 2399–2406.

91. Cook AM, Denger K. Metabolism of Taurine in Microorganisms. In: Oja SS, Saransaari P (eds). *Taurine 6*. 2006. Springer US, pp 3–13.

92. Grein F, Ramos AR, Venceslau SS, Pereira IAC. Unifying concepts in anaerobic respiration: Insights from dissimilatory sulfur metabolism. *Biochimica et Biophysica Acta (BBA) - Bioenergetics* 2013; **1827**: 145–160.

93. Rein U, Gueta R, Denger K, Ruff J, Hollemeyer K, Cook AM. Dissimilation of cysteate via 3-sulfolactate sulfo-lyase and a sulfate exporter in Paracoccus pantotrophus NKNCYSA. *Microbiology*, 2005; **151**: 737–747.

94. Kertesz MA. Riding the sulfur cycle – metabolism of sulfonates and sulfate esters in Gram-negative bacteria. *FEMS Microbiol Rev* 2000; **24**: 135–175.

95. Kleiner M, Wentrup C, Lott C, Teeling H, Wetzel S, Young J, et al. Metaproteomics of a gutless marine worm and its symbiotic microbial community reveal unusual pathways for carbon and energy use. *PNAS* 2012; **109**: E1173–E1182.

96. Lackner G, Peters EE, Helfrich EJN, Piel J. Insights into the lifestyle of uncultured bacterial natural product factories associated with marine sponges. *PNAS* 2017; **114**: E347–E356.

97. Baldock MI, Denger K, Smits THM, Cook AM. *Roseovarius* sp. strain 217: aerobic taurine dissimilation via acetate kinase and acetate-CoA ligase. *FEMS Microbiology Letters* 2007; **271**: 202–206.

98. Lehmann S. Sulfite dehydrogenases in organotrophic bacteria: enzymes, genes and regulation. 2013. University of Konstanz.

99. Woyke T, Teeling H, Ivanova NN, Huntemann M, Richter M, Gloeckner FO, et al. Symbiosis insights through metagenomic analysis of a microbial consortium. *Nature* 2006; **443**: 950–955.

100. Schwalbach MS, Tripp HJ, Steindler L, Smith DP, Giovannoni SJ. The presence of the glycolysis operon in SAR11 genomes is positively correlated with ocean productivity. *Environmental Microbiology* 2010; **12**: 490–500.

101. Steindler L, Schwalbach MS, Smith DP, Chan F, Giovannoni SJ. Energy Starved Candidatus Pelagibacter Ubique Substitutes Light-Mediated ATP Production for Endogenous Carbon Respiration. *PLOS ONE* 2011; **6**: e19725.

102. Tripp HJ, Kitner JB, Schwalbach MS, Dacey JWH, Wilhelm LJ, Giovannoni SJ. SAR11 marine bacteria require exogenous reduced sulphur for growth. *Nature* 2008; **452**: 741–744.

103. Gamagedara S, Shi H, Ma Y. Quantitative determination of taurine and related biomarkers in urine by liquid chromatography–tandem mass spectrometry. *Anal Bioanal Chem* 2012; **402**: 763–770.

104. Shinagawa A, Suzuki T, Konosu S. The Role of Free Amino Acids and Betaines in Intracellular Osmoregulation of Marine Sponges. *Nippon Suisan Gakkaishi* 1992; **58**: 1717–1722.

105. Rix L, Ribes M, Coma R, Jahn MT, de Goeij JM, van Oevelen D, et al. Heterotrophy in the earliest gut: a single-cell view of heterotrophic carbon and nitrogen assimilation in sponge-microbe symbioses. *ISME J* 2020; **14**: 2554–2567.

106. Brüggemann C, Denger K, Cook AM, Ruff J. Enzymes and genes of taurine and isethionate dissimilation in Paracoccus denitrificans. *Microbiology* 2004; **150**: 805–816.

107. Weinitschke S, von Rekowski KS, Denger K, Cook AM. Sulfoacetaldehyde is excreted quantitatively by Acinetobacter calcoaceticus SW1 during growth with taurine as sole source of nitrogen. *Microbiology* 2005; **151**: 1285–1290.

108. Denger K, Smits THM, Cook AM. Genome-enabled analysis of the utilization of taurine as sole source of carbon or of nitrogen by Rhodobacter sphaeroides 2.4.1. *Microbiology* 2006; **152**: 3197–3206.

109. Amin SA, Hmelo LR, van Tol HM, Durham BP, Carlson LT, Heal KR, et al. Interaction and signalling between a cosmopolitan phytoplankton and associated bacteria. *Nature* 2015; **522**: 98–101.

110. Palatinszky M, Herbold C, Jehmlich N, Pogoda M, Han P, von Bergen M, et al. Cyanate as an energy source for nitrifiers. *Nature* 2015; **524**: 105–108.

111. Koch H, Lücker S, Albertsen M, Kitzinger K, Herbold C, Spieck E, et al. Expanded metabolic versatility of ubiquitous nitrite-oxidizing bacteria from the genus *Nitrospira*. *Proc Natl Acad Sci USA* 2015; **112**: 11371–11376.

112. Kitzinger K, Padilla CC, Marchant HK, Hach PF, Herbold CW, Kidane AT, et al. Cyanate and urea are substrates for nitrification by Thaumarchaeota in the marine environment. *Nature Microbiology* 2019; **4**: 234–243.

113. Clifford EL, De Corte D, Amano C, Paliaga P, Ivančić I, Ortiz V, et al. Mesozooplankton taurine production and prokaryotic uptake in the northern Adriatic Sea. *Limnol Oceanogr* 2020; **65**: 2730–2747.

114. Wybouw N, Dermauw W, Tirry L, Stevens C, Grbić M, Feyereisen R, et al. A gene horizontally transferred from bacteria protects arthropods from host plant cyanide poisoning. *eLife* 2014; **3**: e02365.

115. Guedes R, Prosdocimi F, Fernandes G, Moura L, Ribeiro H, Ortega J. Amino acids biosynthesis and nitrogen assimilation pathways: a great genomic deletion during eukaryotes evolution. *BMC Genomics* 2011; **12**: S2.

116. Costa I, Thompson J, Ortega J, Prosdocimi F. Metazoan Remaining Genes for Essential Amino Acid Biosynthesis: Sequence Conservation and Evolutionary Analyses. *Nutrients* 2014; **7**: 1–16.

117. Munroe S, Sandoval K, Martens DE, Sipkema D, Pomponi SA. Genetic algorithm as an optimization tool for the development of sponge cell culture media. *In Vitro CellDevBiol-Animal* 2019; **55**: 149–158.

118. Fitzgerald LM, Szmant AM. Biosynthesis of 'essential' amino acids by scleractinian corals. *Biochemical Journal* 1997; **322**: 213–221.

119. Dassler T, Maier T, Winterhalter C, Bock A. Identification of a major facilitator protein from Escherichia coli involved in efflux of metabolites of the cysteine pathway. *Mol Microbiol* 2000; **36**: 1101–1112.

120. Kutukova EA, Livshits VA, Altman IP, Ptitsyn LR, Zyiatdinov MH, Tokmakova IL, et al. The *yeaS* (*leuE*) gene of *Escherichia coli* encodes an exporter of leucine, and the Lrp protein regulates its expression. *FEBS Letters* 2005; **579**: 4629–4634.

121. Elliott GRD, Leys SP. Evidence for glutamate, GABA and NO in coordinating behaviour in the sponge, Ephydatia muelleri (Demospongiae, Spongillidae). *Journal of Experimental Biology* 2010; **213**: 2310–2321.

122. Ueda N, Richards GS, Degnan BM, Kranz A, Adamska M, Croll RP, et al. An ancient role for nitric oxide in regulating the animal pelagobenthic life cycle: evidence from a marine sponge. *Scientific Reports* 2016; **6**.

123. Cramm R, Pohlmann A, Friedrich B. Purification and characterization of the single-component nitric oxide reductase from *Ralstonia eutropha* H16. *FEBS Letters* 1999; **460**: 6–10.

124. Hendriks J, Oubrie A, Castresana J, Urbani A, Gemeinhardt S, Saraste M. Nitric oxide reductases in bacteria. *Biochimica et Biophysica Acta (BBA) - Bioenergetics* 2000; **1459**: 266–273.

125. Achlatis M, Pernice M, Green K, de Goeij JM, Guagliardo P, Kilburn MR, et al. Single-cell visualization indicates direct role of sponge host in uptake of dissolved organic matter. *Proceedings of the Royal Society B: Biological Sciences* 2019; **286**: 20192153.

126. Leys SP, Kahn AS, Fang JKH, Kutti T, Bannister RJ. Phagocytosis of microbial symbionts balances the carbon and nitrogen budget for the deep-water boreal sponge *Geodia barretti*: Metabolism of *Geodia barretti*. *Limnol Oceanogr* 2018; **63**: 187–202.

127. Deane EM, O'Brien RW. Uptake of sulphate, taurine, cysteine and methionine by symbiotic and free-living dinoflagellates. *Arch Microbiol* 1981; **128**: 311–319.

128. Wang JT, Douglas AE. Nutrients, Signals, and Photosynthate Release by Symbiotic Algae (The Impact of Taurine on the Dinoflagellate Alga Symbiodinium from the Sea Anemone Aiptasia pulchella). *Plant Physiology* 1997; **114**: 631–636.

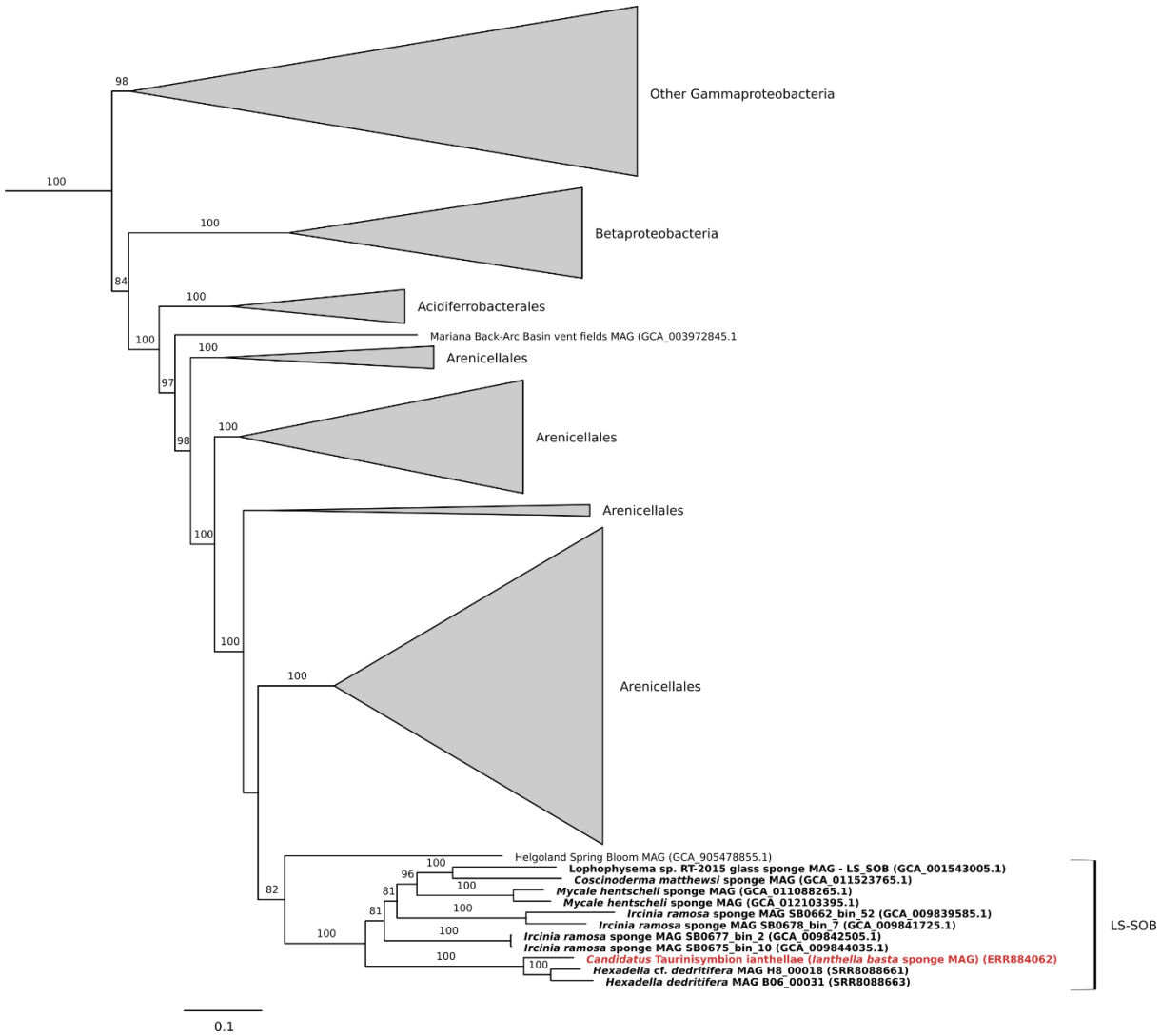

Figure 1. Maximum-likelihood phylogenomic tree (after automatic model selection with IQ-Tree) of '*Ca*. Taurinisymbion ianthellae' (red and bold) along with other selected proteobacterial symbionts (sponge symbionts in bold font). The phylogenomic tree is based on 43 concatenated universal, single-copy marker genes identified with CheckM.

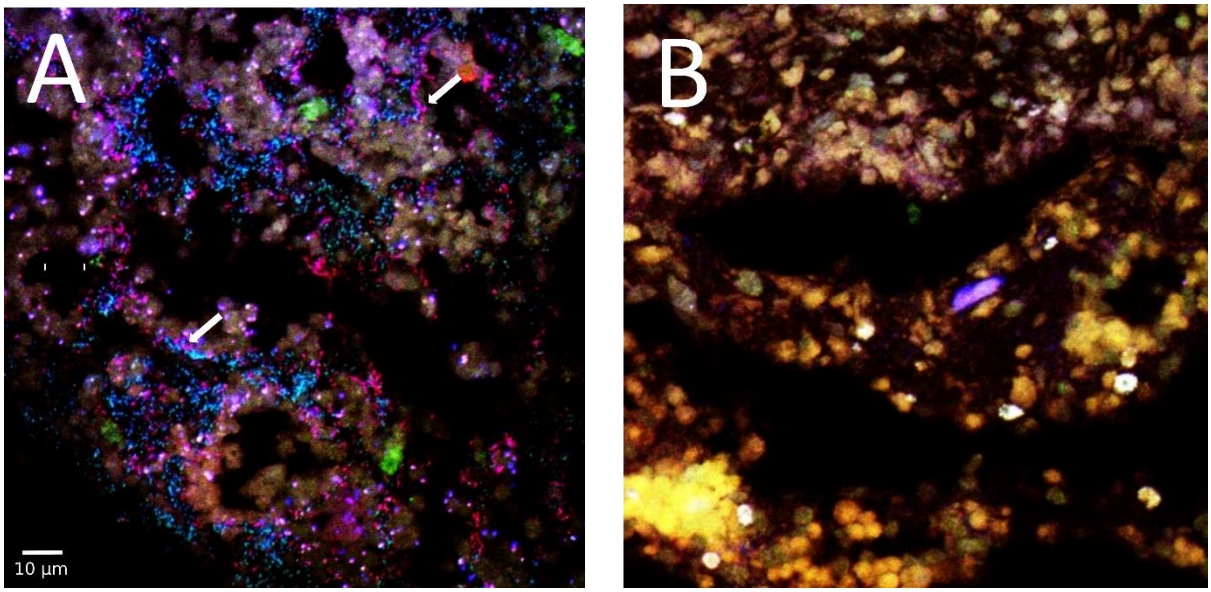

Figure 2. Fluorescence *in situ* hybridization of 5 µm thick cryo-sections of *Ianthella basta* using double-labeled probe sets [55]. A) '*Ca.* Taurinisymbion ianthellae' (red), *Alphaproteobacteria* symbiont-probe (green), and *Bacteria*-probe (EUB338-I-III; blue); B) negative controls using the double-labeled non-EUB338 probe set are depicted in all three color channels. The combination of the '*Ca.* Taurinisymbion ianthellae' specific probe signals in red with the general *Bacteria* probe signals in blue, results in the visualization of '*Ca.* Taurinisymbion ianthellae' as magenta signals and representative cells are indicated with white arrows. The α-symbiont appears in cyan. Green structures represent autofluorescence.

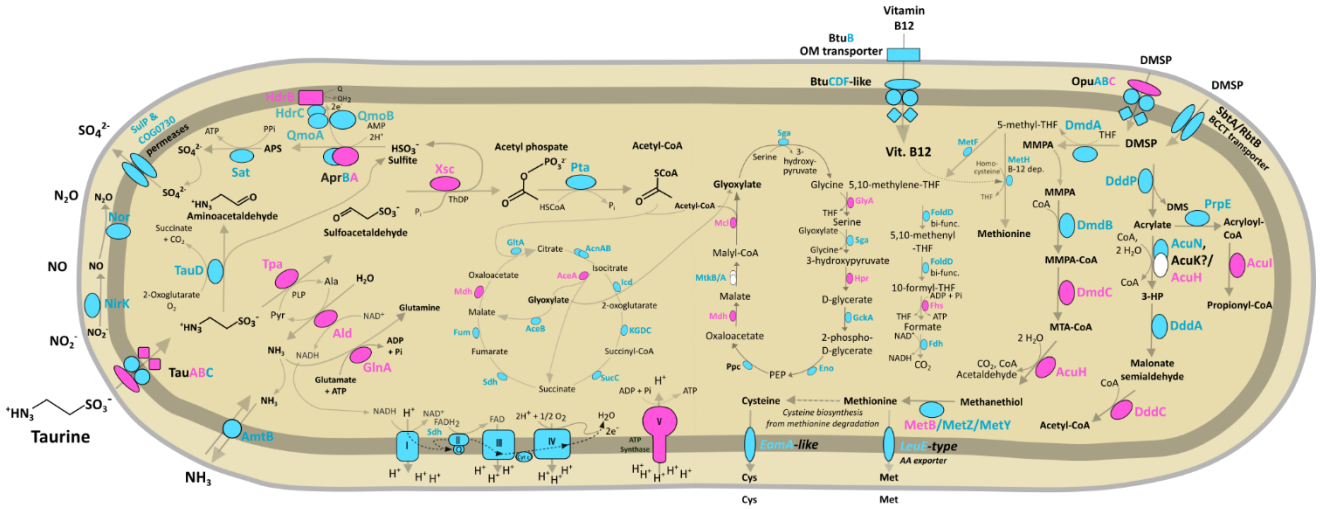

Figure 3. Taurine and DMSP metabolic pathways identified and expressed in '*Ca.* Taurinisymbion ianthellae'. Central carbon and nitrogen metabolism in '*Ca.* Taurinisymbion ianthellae' based on metaproteogenomic analyses with a focus on taurine and DMSP metabolism pathways along with the relevant import and export of exchanged metabolites. Depicted are proteins necessary for taurine import, followed by taurine dissimilation, energy conservation via sulfite oxidation and the electron transport chain, along with carbon incorporation via the glyoxylate bypass. Similarly depicted are the proteins necessary for DMSP import as well as the corresponding DMSP cleavage and demethylation pathways, including the oxidation of 5-methyl-THF and its role as a carbon donor for the conversion of glycine to serine. Enzymes detected via metaproteomics are highlighted in pink, while enzymes only identified in the '*Ca.* Taurinisymbion ianthellae' MAG are highlighted in turquoise. Missing pathway genes are depicted as white shapes. AMP, adenosine monophosphate; APS, adenosine-5'-phosphosulfate, Cys, cysteine; DMSP, dimethylsulfoniopropionate; DMS, dimethylsulfide; 3-HP, 3-hydroxypropanoate; Met, methionine; MMPA, methylmercaptopropionate; MTA-CoA, methylthioacryloyl-Coenzyme A; PEP, phosphoenolpyruvate; PLP, pyridoxal 5'-phosphate; Q, quinone; ThDP, thiamine diphosphate; THF, tetrahydrofolate. Additional information for genes and pathways depicted in the figure can be found in Supplemental Tables S2-S5.

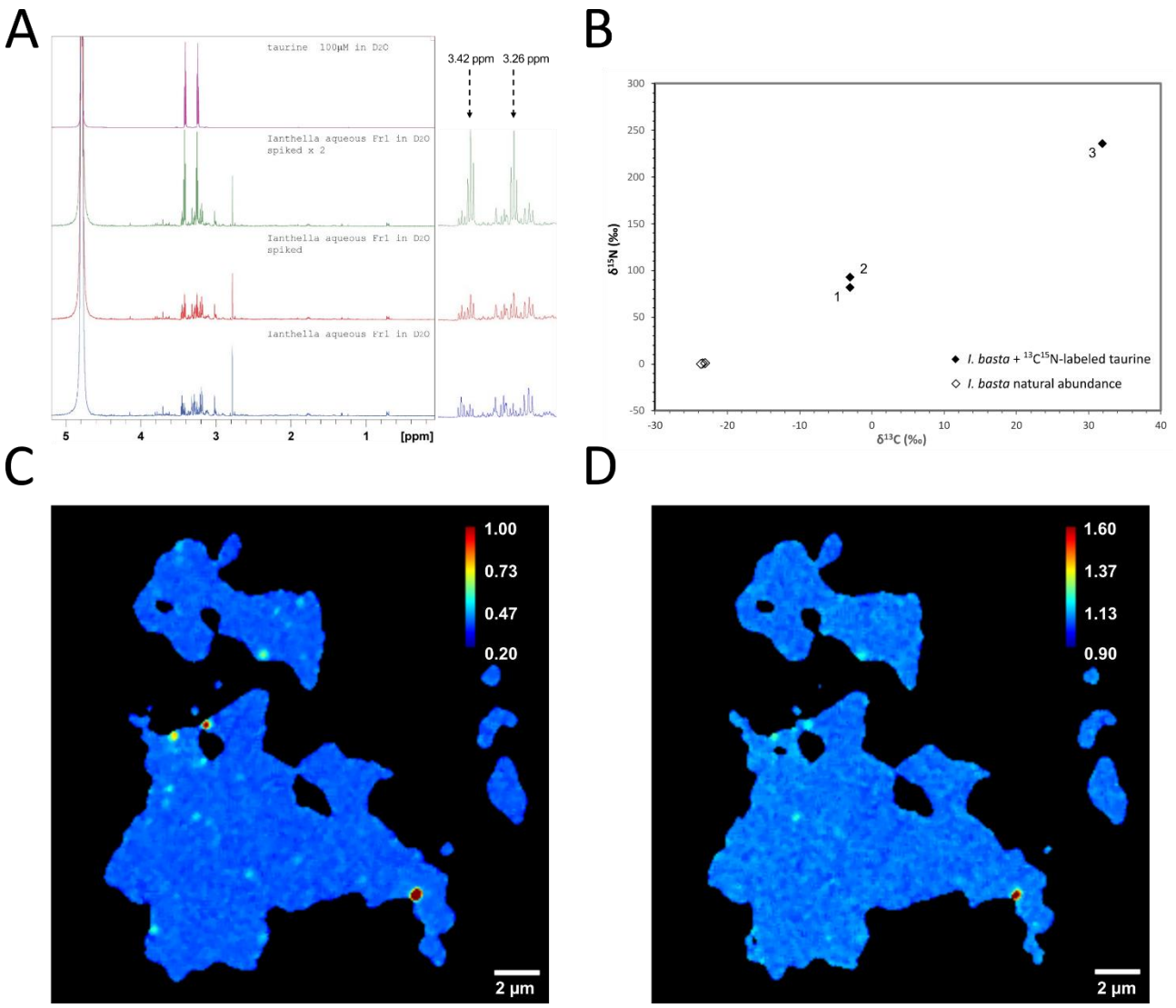

Figure 4. (A) Detection of taurine in the aqueous fraction Fr1 of the 90% methanol extract of *Ianthella basta* via ^{1}H NMR. ^{1}H NMR spectra of Fr1 from C18 of crude methanolic extract (blue), Fr1 spiked with 32 µL (red) and 128 µL (green) of 100 µM taurine, as well as 100 µM taurine (purple), all acquired in D_2O. Zoomed regions are depicted of diagnostic triplet signals at 3.26 and 3.42 ppm, and the increase in taurine signal intensity with spiking. (B) Incorporation of ^{13}C- and ^{15}N-labeled taurine into sponge holobiont biomass at the total nucleic acid level as determined by EA-IRMS. Data from three sponge clones incubated with labeled taurine (numbered for reference) and three control sponge clones incubated with unlabeled taurine are depicted. (C, D) Incorporation of taurine-derived ^{15}N and ^{13}C into microbial-sized cells as detected by NanoSIMS analysis of extruded extracellular matrix from *I. basta* holobiont samples after incubation with ^{15}N/^{13}C labeled taurine over a period of 48 h. The displayed images were acquired at an erosion depth below the surface of the sample, visualizing the presence of isotopically enriched compounds within the sponge extracellular matrix. Isotope label contents are displayed as isotope fractions on a rainbow color scale, ranging from 0.2 to 1.0 at% ^{15}N and 0.9 to 1.6 at% ^{13}C. Individual values, obtained from region of interest (ROI) specific numerical data evaluation, are displayed in Fig. S6.

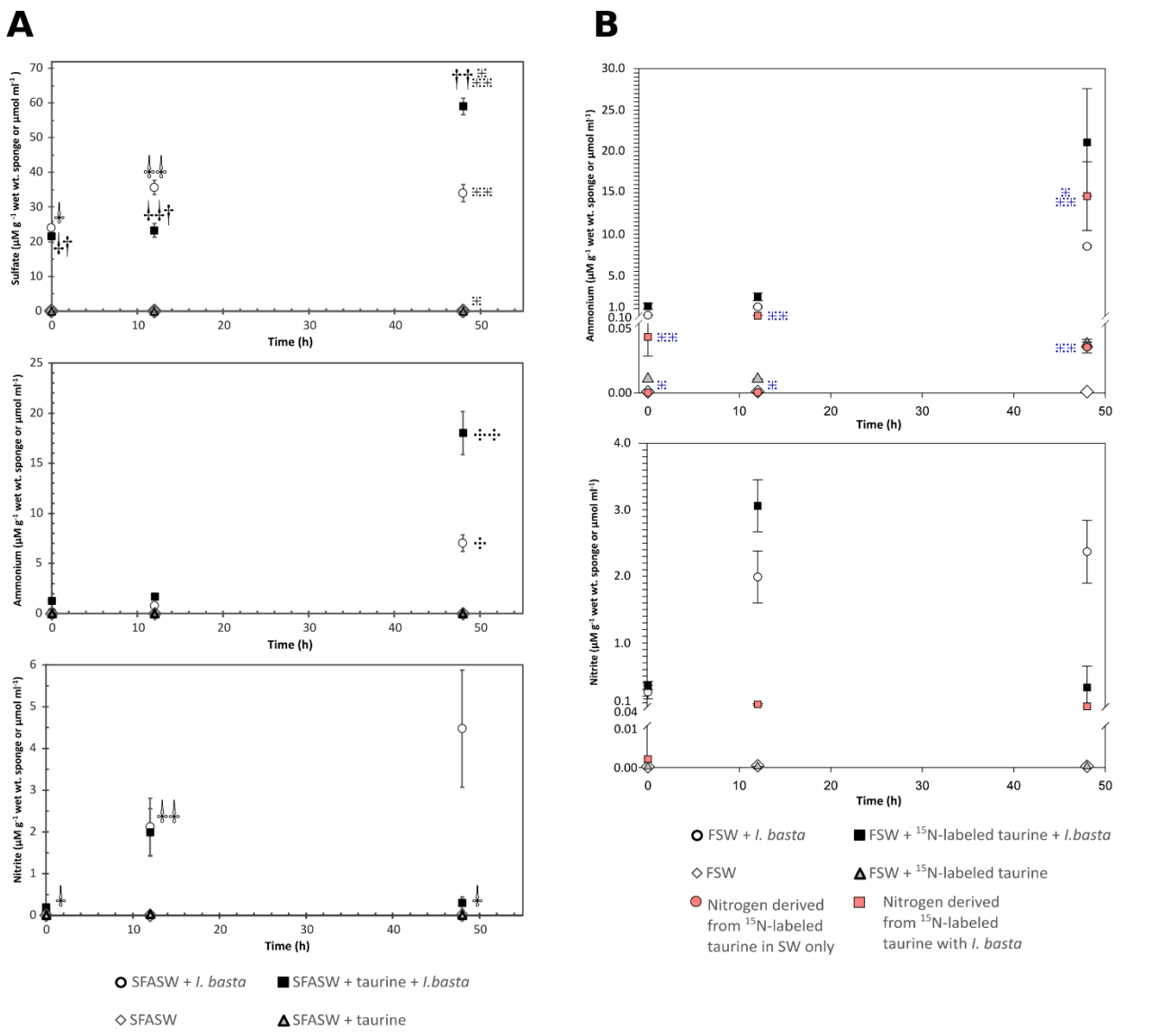

Figure 5. (**A**) Time series of the concentrations of dissolved sulfate, ammonium, and nitrite in the incubation media of *I. basta* holobiont batch incubations (A) 48 h incubation in sulfate-free artificial seawater (SFASW) performed either without (white circle) or with added unlabeled taurine (filled square: t = 0, +1 mM taurine; t = 36 h, +0.6 mM taurine). Concentrations are normalized to the wet weight of the respective *I. basta* clones applied in the incubations (8.83 ± 2.38 SD g wet wt.; range: 6.5 – 13.4 g wet wt.). The data from the corresponding control experiments with SFASW without *I. basta* holobiont are displayed as white diamonds (without added taurine) and grey triangles (with added taurine) and plotted on the same axes, given in µmol ml^{-1}. A starting average concentration of 0.2 mM sulfate was measured in all incubation treatments containing *I. basta* clones most likely representing residual carryover from the sponge material. Incubations were performed in biological triplicates and water samples from each incubation were taken at each time point. In A), ⸸⸸ symbols for sulfate concentrations denote significant difference in pairwise comparisons of incubations from t = 0 (⸸) to t = 12 (⸸⸸) for both the incubations with *I. basta* and taurine and without added taurine ($p < 0.05$, one-tailed t-test); †† symbols in the sulfate concentration panel reflect significant differences for sulfate concentrations for *I. basta* and taurine incubations at t = 48 (††) when compared to the earlier time points (†) (one-way ANOVA followed by Holm-Sidak tests, $p < 0.001$); similarly, the number of ⌘ symbols reflects significant differences for sulfate concentrations for incubations with *I. basta* and taurine when compared to all other treatments at t = 48 h (one-way ANOVA followed by Holm-Sidak tests, $p < 0.001$). ⌖⌖ in the ammonium concentration panel reflects

a significant difference between incubations with *I. basta* and taurine and only *I. basta* (⁜)(two-tailed t-test, $p < 0.05$). ⸸⸸ in the nitrite concentration panel reflects a significant difference between time points for the incubations with *I. basta* and taurine (one-way ANOVA followed by Tukey pairwise multiple comparison tests, $p < 0.05$). (**B**) Ammonium and nitrite accumulation in *I. basta* holobiont batch incubations (48 h) in natural filtered seawater (FSW) performed either with added taurine (filled symbols: t = 0, +1 mM taurine; t = 36 h, +0.6 mM taurine) or without added taurine (9.45 ± 2.53 SD g wet wt.; range: 5.5 – 12.7 g wet wt.). Taurine was added as an equimolar mixture of ^{13}C- and ^{15}N-labeled taurine to obtain sponge material for subsequent EA-IRMS and NanoSIMS analyses (by sacrificially sampling sponges at the end of the experiment) as well as to measure ^{15}N in NH_4^+ and NO_2^-. Incubations were performed in biological triplicates and water samples from each incubation were taken at each time point. The data from the corresponding control experiments with FSW without *I. basta* holobiont are displayed as white circles and diamonds as in A). Pink symbols represent the measured concentrations of ^{15}N in ammonium and nitrite that were a product of the added ^{15}N-labeled taurine (t = 0, +0.5 mM ^{15}N-labeled taurine; t = 36 h, +0.3 mM ^{15}N-labeled taurine). The number of ⁜ symbols in the ammonium concentration panel in B) reflects significant differences in $^{15}NH_4^+$ concentrations measured in incubations with *I. basta* and isotopically labeled taurine and in incubations without *I. basta* between different time points and across treatments (one-way ANOVA followed by Student-Newman-Keuls pairwise multiple comparison tests, $p < 0.05$). Error bars refer to +/- 1SE.

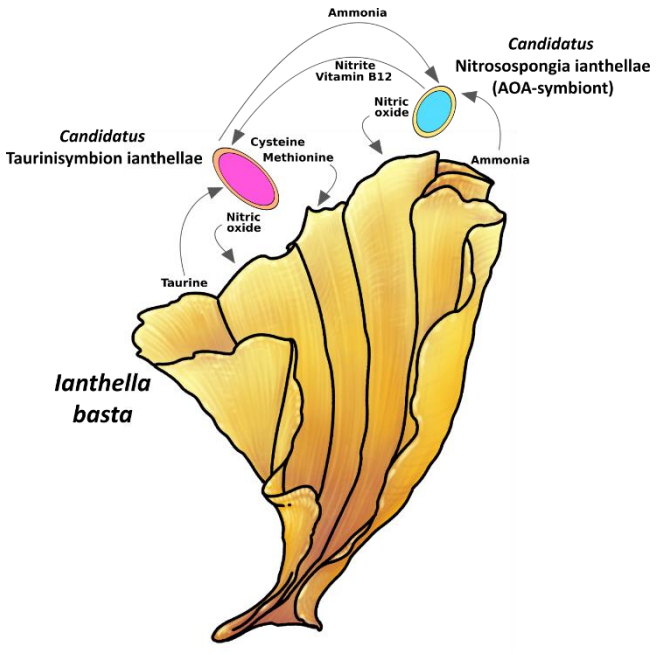

Figure 5. Conceptual scheme of tripartite metabolic interactions within the *I. basta* holobiont.